Final Report for AOARD Grant # FA2386-12-1-4002

"Nanofluidic Pre-Concentration Devices for Enhancing the Detection Sensitivity and Selectivity of Biomarkers for Human Performance Monitoring"

December 1, 2012

Name of Principal Investigators (PI and Co-PIs): Chia-Fu Chou
- E-mail address: cfchou@phys.sinica.edu.tw
- Institution: Academia Sinica
- Mailing Address: Institute of Physics, 128, Sec. 2, Academia Rd., Nankang, Taipei 11529, Taiwan
- Phone: +886-2-2789-6761
- Fax: +886-2-2651-0704

Period of Performance: 11/28/2011 – 11/27/2012

Abstract:
Mass transport has generally been recognized as a major limiting factor in the sensitivity and performance of miniaturized sensor platforms. To overcome this limitation, a new approach, termed *molecular dam*, has been developed to enhance mass transport for protein enrichment in nanofluidic channels by nanoscale electrodeless dielectrophoresis under physiological buffer conditions. We demonstrated protein enrichment factor to be greater than 10^5-fold in 20 seconds, which is orders of magnitude faster than most reported methods. We also studied the detailed mechanism as how the electrokinetic forces get balanced to achieve the molecular damming effect and the scaling relation of force and nanoconstriction size. Both the capillary- and electrokinetically-driven nanoslit sensor platforms have also been developed in parallel to enhance the reaction kinetics of protein sensing by reducing the diffusion length of reactants.

Introduction:
A methodology for the real-time assessment of a diverse set of performance biomarkers, which are indicators of fatigue, vigilance, and stress, is currently being undertaken by the 711th Human Performance Wing at the Wright Patterson Air Force Base to assess the preparedness of its personnel for various missions. However, the current sensor platform is unable to sensitively monitor these biomarkers within real biological fluid media such as saliva and blood, due to the presence of interfering proteins at far higher levels. The specific aim of this project is to develop devices for both the capillary- (no energy consumption) and electrokinetically-driven nanoslit sensors of relevant neuropeptide biomarkers, so that their levels can eventually be monitored in biological fluids. This project is to be performed with joint effort in University of Virginia led by Prof. Nathan Swami and in University of Notre-Dame led by Prof. Hsueh-Chia Chang. The collaborative effort with Prof. Swami's lab is on the development of nanofluidic protein enrichment devices to be integrated later with the nanoslit platform for enhancing the detection sensitivity and selectivity of biomarkers for human performance monitoring. The Year 1 Quarterly Milestones are listed below which have been achieved during the 1st year of this project.

Year 1 Quarterly Milestones	Q1	Q2	Q3	Q4
1. Functionalization and fabrication of biofunctional nanoslits with built-in capillary pump	■	■		
2. Testing capillary-driven nanoslit device with model protein binding assay (streptavidin-avidin) using fluorescence imaging		■		
3. Functionalization and fabrication of biofunctional nanoslits with electrokinetic pump		■	■	
4. Testing electrokineticly-driven nanoslit device with model protein binding assay (streptavidin-avidin) using fluorescence imaging			■	
5. Fabrication of anti-body-functionalized nanoslits			■	■
6. Testing both electrokineticly-driven nanoslit device with antibody-antigen binding assay (IgG−anti-IgG) using fluorescence imaging				■

In years 2-3, we envision collaborations with scientists at the Air Force Base in the development of an

Report Documentation Page

Form Approved
OMB No. 0704-0188

1. REPORT DATE	2. REPORT TYPE	3. DATES COVERED
03 DEC 2012	**Final**	**01-12-2011 to 02-12-2012**

4. TITLE AND SUBTITLE
Nanofluidic Pre-Concentration Devices for Enhancing the Detection Sensitivity and Selectivity of Biomarkers for Human Performance Monitoring

5a. CONTRACT NUMBER
FA23861214002

5b. GRANT NUMBER

5c. PROGRAM ELEMENT NUMBER

6. AUTHOR(S)
Chia-Fu Chou

5d. PROJECT NUMBER

5e. TASK NUMBER

5f. WORK UNIT NUMBER

7. PERFORMING ORGANIZATION NAME(S) AND ADDRESS(ES)
Academia Sinica,128 Sec 2 Academia Rd Nankang Dist,Taipei 11529,Taiwan,TW,11529

8. PERFORMING ORGANIZATION REPORT NUMBER
N/A

9. SPONSORING/MONITORING AGENCY NAME(S) AND ADDRESS(ES)
AOARD, UNIT 45002, APO, AP, 96338-5002

10. SPONSOR/MONITOR'S ACRONYM(S)
AOARD

11. SPONSOR/MONITOR'S REPORT NUMBER(S)
AOARD-124002

12. DISTRIBUTION/AVAILABILITY STATEMENT
Approved for public release; distribution unlimited

13. SUPPLEMENTARY NOTES

14. ABSTRACT
Mass transport has generally been recognized as a major limiting factor in the sensitivity and performance of miniaturized sensor platforms. To overcome this limitation, a new approach, termed molecular dam, has been developed to enhance mass transport for protein enrichment in nanofluidic channels by nanoscale electrodeless dielectrophoresis under physiological buffer conditions. The researchers demonstrated protein enrichment factor to be greater than 105-fold in 20 seconds, which is orders of magnitude faster than most reported methods. They also studied the detailed mechanism as how the electrokinetic forces get balanced to achieve the molecular damming effect and the scaling relation of force and nanoconstriction size. Both the capillary- and electrokinetically-driven nanoslit sensor platforms have also been developed in parallel to enhance the reaction kinetics of protein sensing by reducing the diffusion length of reactants.

15. SUBJECT TERMS
Biomarkers, Nanofluidics, Pre-concentration Devices, Sensing

16. SECURITY CLASSIFICATION OF:			17. LIMITATION OF ABSTRACT	18. NUMBER OF PAGES	19a. NAME OF RESPONSIBLE PERSON
a. REPORT	b. ABSTRACT	c. THIS PAGE			
unclassified	**unclassified**	**unclassified**	**Same as Report (SAR)**	**41**	

integrated multi-modal sensor platform for multiple biomarker target detection for effectively monitoring the mission preparedness of its personnel, which includes initial detection of Orexin and other pertinent biomarkers in nanoslit using fluorescence imaging, obtain kinetic curves for titration of various Orexin concentrations, develop testing nanoslit devices for spiked samples, and test nanoslit devices for clinical samples.

Experiments: Description of the experiment(s)/theory and equipment or analyses.

1. Functionalization and fabrication of biofunctional nanoslits with built-in capillary pump

A single biofunctional nanoslit was fabricated with a depth of 50 nm, followed by immobilizing the patches of chemical ligands (biotin) using typical photolithography procedure. The nanoslit was connected to periodic structures which carry the protein (streptavidin conjugated with Alexa Fluor 488, abbreviated as Streptavidin-488) solution flowing through the biosensor area. The immobilized biotin patches were used as biosensors to capture the streptavidin-488 in the sample solution.

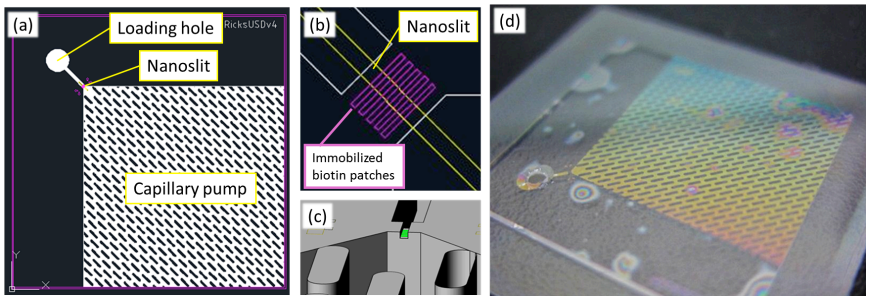

Figure 1. The schematics of the biofunctional nanoslits with built-in capillary pump.(a) Streptavidin-488 solution was loaded to the loading hole. Using the capillary pumping structures, streptavidin-488 were captured when aqueous solution flow through the biotin patterns in the nanoslit. (b,c)The close look of the design of biotin patches and the nanoslit. (d) The chip of biofunctional nanoslits with the capillayr pump structure.

2. Testing capillary-driven nanoslit device with model protein binding assay (streptavidin-biotin) using fluorescence imaging.

Streptavidin-488 was used as a model protein to reveal the real-time spatial distribution of the binding reaction. In figure 2, 1 nM of streptavidin-488 solution was introduced, and carried into the nanoslit biosensor without external pump. Linear flow rate were estimated to be 25 μm/s. Fluorescence signal on the first sensor area could be distinguished after eight minutes, and reached equilibrium after around 30 minutes.

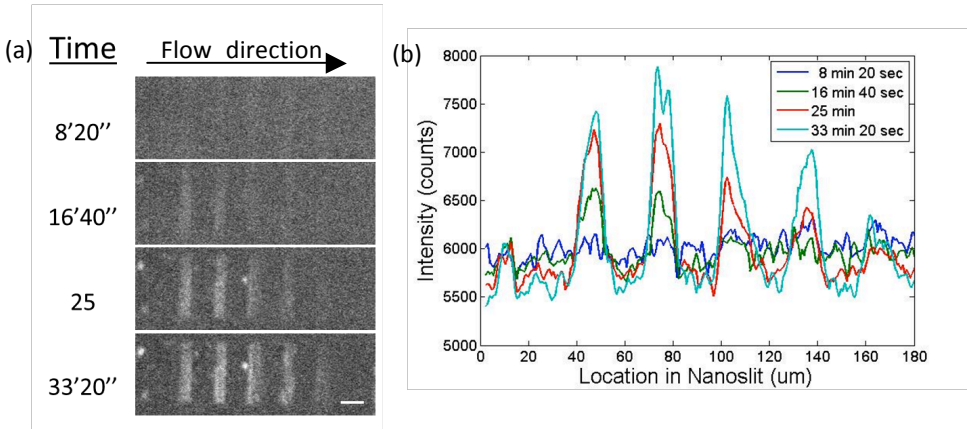

Figure 2. The real-time binding reaction kinetics of nanoslit biosensor with built-in capillary pump. (a) The fluorescence time-lapse imaging of 1 nM streptavidin-488 binding onto the immobilized biotin patches. Scale bar represents 20 um. (b) The line plot of the fluorescence intensity along the center of the nanoslits.

3. Functionalization and fabrication of biofunctional nanoslits with electrokinetic pump and testing electrokinetically-driven nanoslit device with model protein binding assay (streptavidin-biotin) using fluorescence imaging.

Electrokinetic flow is shown to be effective for analyte transport, especially in nano/microfluidic devices. Therefore, we fabricated a nanoslit with immobilized biotin array, conjugated to microchannels and external electrodes. For 100 nM of streaptavidin-488, the first sensor area starts to show significant fluorescence response after 4 minutes and reaches equilibrium after around 6 minutes. Using fluorescence imaging, the spatial distribution of protein binding events was recorded in real-time. As in figure 4, electrokinetic flow increases the binding events around ~230 fold comparing to simple diffusion in the nanoslit, and almost reaches equilibrium in around 4 minutes. A notable phenomenon is that when the first sensor area is reaching its equilibrium fluorescence intensity at around 25,000 counts, the second patch shows merely around 4,000 counts, and the third to fifth patches were less than 2,000 counts. This demonstrates the power of high capturing efficiency of the nanoslit biosensors.

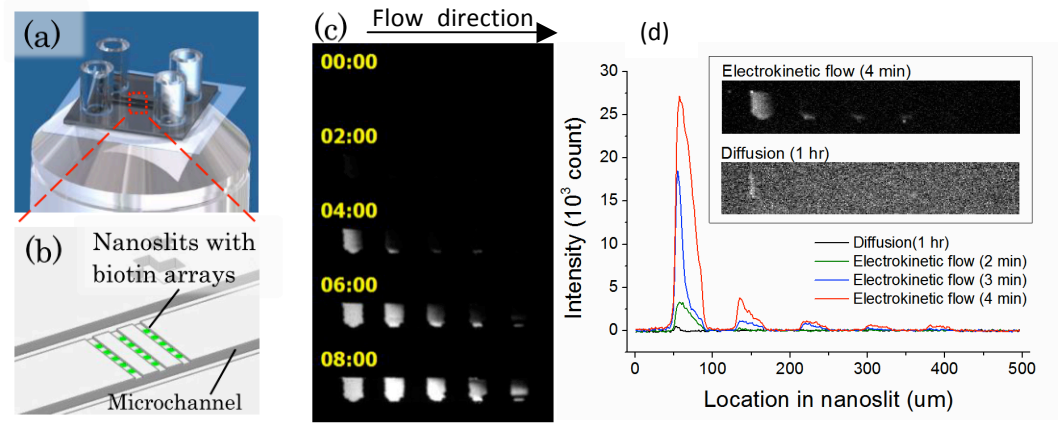

Figure 3. Schematics of the nanoslit biosensor chip. (a) Overview of the chip setup. Voltage was applied through the four reservoirs. Fluorescence images were taken through the objective in the bottom. (b) Three nanoslits were placed in-between two microchannels, and were immobilized with biotin patterns (green). (c) Images taken by time-lapse fluorescence microscopy. 100 nM of Alexa Fluor 488-streptavidin was driven into nanoslit by electroosmotic flow with applied field of 200V/cm. (d) Protein binding kinetics visualized by fluorescence imaging. (insert) 100 nM of Alexa488-streptavidin solution was loaded and driven into nanoslit protein sensor patches by diffusion or electrokinetically driven flow. Intensities in the center area along nanoslits (yellow dashed line) was extracted and plotted.

4. Fabrication of anti-body-functionalized nanoslits and test the electrokinetically-driven nanoslit device with antibody-antigen binding assay (IgG versus anti-IgG) using fluorescence imaging.

For the antibody immobilization process, the chips were etched for microfluidic channels structures and pre-modified with epoxy-silane, which served as a linker to covalently conjugate to the antibodies. Microarray spotter machine was used to spatially allocate antibodies onto designed location on the chip, and the microfluidic devices were encapsulated immediately after the spotting. Chips were stored in 4°C for later use. In figure 5, microchannels were pre-wetted with PBS and later loaded with PBS containing fluorescence IgG-DyLight 488 (0.15mg/mL) and BSA (1.5 mg/mL) and driven by an electric field of 200V/cm. As shown in figure 5, the fluorescence started to increase after 30 seconds, and reached equilibrium after 90 seconds on the first spot. Furthermore, all the three spots reached their equilibrium after around 150 seconds. Notably, at 90 seconds, the second and third patches showed significant darkness, which should be resulted from the high capturing efficiency of the first spot, which consumes most of the IgG-DyLight 488 flowing through.

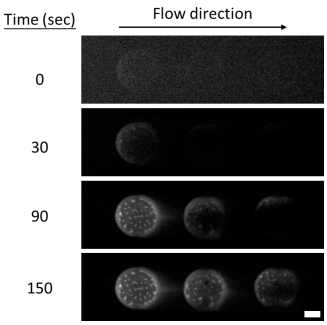

Figure 4. Binding kinetics of IgG-DyLight 488 (0.15 mg/mL) captured by the surface immobilized antibodies in microchannel of 1.1 μm depth. The electric field was 200 V/cm, and the scale bar represents 50 μm.

5. Molecular damming device with nanoconstrictions for ultrafast protein enrichment.

The concept of molecule dam has been proposed and device fabricated to demonstrate highly efficient protein enrichment. Dielectric nanoconstrictions, down to 30 nm in size, embedded in nanofluidic device, serve as field focusing lens capable of magnifying the applied field to 10^5-fold when combined with a micro-to-nanofluidic step interface. Empowered by this strong field and the associated field gradient occurred at the nanoconstrictions, we demonstrate proteins are enriched by molecular damming effect, faster than the trapping effect, to greater than 10^5-fold in 20 seconds.

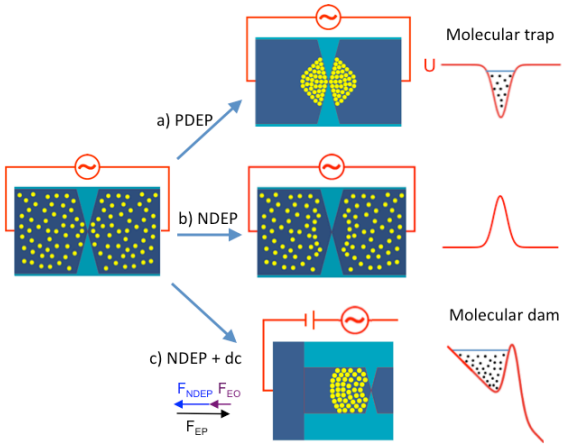

Figure 5. The concept of nanoscale molecular trap and dam. When an ac electric field is applied across a nanoconstriction, composed of a pair of sharp insulating tips with a constriction gap of 10's nm apart embedded in a sealed channel, the field can be highly focused and a strong field gradient is generated for the operation of (a) positive dielectrophoresis (PDEP) or (b) negative dielectrophoresis (NDEP), if the dielectric permittivity of an analyte (shown in dots) is larger or smaller than that of the medium, respectively. The attractive potential in (a) serves as a molecular trap, while the repulsive potential in (b) keeps molecules away from the constriction. However, if a dc bias is applied in the case of NDEP, as shown in (c) for negatively charged particles, it tilts the repulsive potential into a slanted well, where the force balance condition, $F_{EP}=F_{EO}+F_{NDEP}$, occurs at local potential minimum, which could then cause protein accumulation in a continuous fashion, effectively working as a molecular dam.

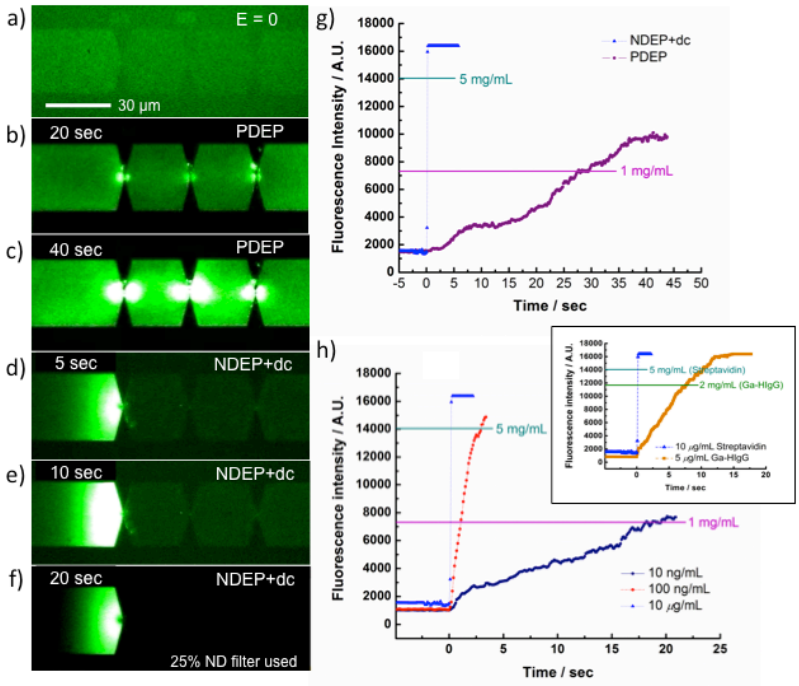

Figure 6. Demonstration of protein trapping and damming with na-noscale eDEP. (a) Proteins (Alexa-488 labeled streptavidins, 10 μg/mL) loaded in the chip by capillary force. Protein trapping with PDEP at (b) 20 s and (c) 40 s after 473 Vpp/cm ac field applied across the chip at 10 KHz. This field is focused 7x104 fold (~3.3x109 Vpp/m) over the applied field at the constrictions. All three constrictions show trapping of strep-tavidins, indicating PDEP is at work. (d)-(f): Protein damming is demonstrated by NDEP+dc: the ac field of 214 Vpp/cm is applied at 1 MHz with 1.5 V/cm dc bias (with positive potential at the right side of the channel). In (f), the image was taken with a 25% transmittance neu-tral density (ND) filter to keep the intensity below the saturation of the EMCCD. The dark zone at the center of the first constriction indicates NDEP is at work where streptavidins are repelled away. It is noted that there are virtually no excessive molecules to go beyond the first dam, before reaching its saturation, for an effective accumulation at the sec-ond and third dams around the constrictions to show the same dark zone as at the first constriction with good contrast. (g) The corresponding intensity plot of protein enrichment, at the same initial concentration of 10 μg/mL, operated under the same experimental conditions of molecu-lar trapping and damming above. The plateau in the damming curve means the EMCCD has reached saturation, where an extended intensity plot with the use of ND filter is shown in Figure S2. (h) Protein enrich-ment curves for various initial concentrations (10 ng/mL or 189 pM, 100 ng/mL, and 10 μg/mL) when operated under molecular damming effect with corresponding dc bias of 1.5, 4.5, and 1.5 V/cm. The concentration rulers of streptavidin are drawn as horizontal lines. Note that 10 ng/mL proteins are enhanced >105 fold in less than 20 seconds. The inset in (h) shows the damming of Alexa-488 labeled goat anti-human IgG, which reaches 400-fold enrichment in 7.5 s from a concentration of 5 μg/mL (33 nM), against Alexa-488 streptavidins (500-fold enrichment in < 1 s) under the same applied field conditions as in (d)-(f).

Results and Discussion:

Within nanoslits, target biomolecules are effectively confined to the surfaces, thus enhance the binding reactions on embedded sensors. Intuitively, the reduced diffusion time should shorten the response time. However, literatures applying the protein nanofluidic sensors rely on the channel electric impedance measurement display response times usually longer than an hour. To characterize and optimize the performance of nano-biosensors, it is crucial to visualize the binding process on sensors in real-time and with good spatial resolution, instead of measuring the averaged signal changes across the nanochannels. In this study, we investigated the fast binding kinetics of proteins inside nanofluidic slits due to the reduction of diffusion length dictated by the slit height. Furthermore, the use of electrokinetic flow is shown to be effective for analyte transport compared to pressure-driven flow in nanoslits despite the high fluid resistance. Our results present a platform that enables visualization of the reaction kinetics in nanofluidic channels with potential applications in kinetics study and clinical diagnostics. In the 2nd year of this project, we aim to implement the thrombin aptamer sensors, obtained from Air Force Research Lab, in the nanoslit to verify the immobilization protocol and sensing kinetics for later applications to human performance biomarkers detection from AFRL. The 3rd year we are to integrate protein enrichment scheme with molecular dams embedded in nanoslit for enhanced sensing of these performance biomarkers.

List of Publications and Significant Collaborations that resulted from your AOARD supported project: In standard format showing authors, title, journal, issue, pages, and date, for each category list the following:

a) Papers published in peer-reviewed journals,

1. K.T. Liao, C.F. Chou*, "Nanoscale molecular traps and dams for ultrafast protein enrichment in high-conductivity buffers", ***J. Am. Chem. Soc.*** **(Comm.)** 134 (21)**,** 8742−8745 (2012). DOI:10.1021/ja3016523 (Featured in ***JACS Spotlights*****:** ***J. Am. Chem. Soc.*** 2012, 134, 10307. DOI:10.1021/ja305430t)
2. K.T. Liao, C. Polanco, V. Chaurey, C.F. Chou*, N.S. Swami*, "Nano-constriction device for rapid protein pre-concentration through balance of electrokinetic forces", ***Electrophoresis*** 33, 1958-1966 (2012)**.** DOI:10.1002/elps.201100707
3. V. Chaurey, A. Rohani, Y.H. Su, K.T. Liao, C.F. Chou*, N.S. Swami*, "Scaling down constriction-based (electrodeless) dielectrophoresis devices for trapping nanoscale bio-particles in physiological media of high-conductivity", ***Electrophoresis***, in press (2012).

b) Papers published in peer-reviewed conference proceedings (N/A),

c) Papers published in non-peer-reviewed journals and conference proceedings (N/A),

d) Conference presentations without papers,

1. C.-F. Chou (2012). "A Decade-Long Advances in Electrodeless Dielectrophoresis (Edep) and Its Future Bioanalytical and Biomedical Applications", ***19th International Symposium on Electro- and Liquid Phase Separation Techniques (ITP 2012)*****,** Sep. 30-Oct. 3, 2012, Baltimore, USA. (Invited Talk)

e) Manuscripts submitted but not yet published (N/A), and

f) Provide a list any interactions with industry or with Air Force Research Laboratory scientists or significant collaborations that resulted from this work.
We have been in close communication with the Air Force Research Laboratory scientist at Wright Patterson Air Force Base, Dr. Jorge Chavez Benavides, in the design and testing of the thrombin aptamer sensors as preliminary study for the later detection of Orexin and other pertinent performance biomarkers.

Attachments: Publications a), b) and c) listed above if possible.
Attached.

DD882: As a separate document, please complete and sign the inventions disclosure form.

JACS
JOURNAL OF THE AMERICAN CHEMICAL SOCIETY
Spotlights
pubs.acs.org/JACS

Spotlights on Recent *JACS* Publications

PHYSICOCHEMICAL CLUES TO GENE FUNCTION

Messenger RNA (mRNA) and transfer RNA (tRNA) are essential molecules in protein-production machinery: mRNA serves as the molecular blueprint that guides protein production, and tRNA translates mRNA into proteins by joining amino acids according to the mRNA sequence. Chemist Bhyravabhotla Jayaram and graduate student Garima Khandelwal have developed a computational method based on DNA's physicochemical properties that can predict whether a gene sequence codes an mRNA or tRNA, without the need for structural data (DOI: 10.1021/ja3020956).

The researchers gathered more than 1,500 prokaryotic genomes from public databases, with more than 2 million mRNA and 50,000 tRNA sequences. They used solvation energy as a measure of DNA's ability to interact with water and calculated for each genome the average solvation energy for each pair of neighboring nucleotides of all RNA sequences in that genome.

tRNA solvation energy values are distinctly higher than and readily differentiated from those of mRNAs when comparing the relative solvation energies for all of the RNAs in each of the genomic sequences. This computational analysis of the physicochemical characteristics of the gene sequences reflects the final structures for which they code—tRNAs are stable structures and less-well solvated than mRNAs. This solvation energy analysis offers a new tactic to identify tRNA-coding regions in a genome sequence without needing tRNA's final structure, bringing a new tool to gene-function studies. **Kenneth J. Moore**

COOPERATION YIELDS GREAT RETURNS

Yonggui Robin Chi and co-workers combine both N-heterocyclic carbenes (NHCs) and Lewis acids, effecting cooperative catalysis in order to cleave C−H bonds up to three carbons away from an aldehyde activating group (DOI: 10.1021/ja303618z). NHC catalysis has more commonly been used to functionalize bonds zero, one, or two carbons away from this type of activating group.

Chemical compounds that could be useful in synthetic, analytical, or other practical applications may have reactive and readily functionalized activating groups, as well as less reactive portions of the molecule. A poorly reactive C−H group, for example, may need to be functionalized to make the compound more useful, but this reaction can be difficult when the bond is remote to the activating group.

Using an NHC in combination either with the Lewis acid scandium(III) triflate alone or with magnesium(II) triflate as well, the researchers were able to activate a carbon three positions away from the activating group. After further reaction, they constructed 6-membered lactone rings that are important flavor and aroma constituents in many natural products. The authors were able to achieve good stereochemical control, and they suggest that this cooperative catalysis technique might be useful for selectively and asymmetrically modifying other molecules. **Christen Brownlee**

MOLECULAR DAMS SPEED UP PROTEIN ENRICHMENT

Miniaturized systems that rapidly detect minute quantities of biological molecules with great sensitivity could be game-changers in medical science. These micro- and nanoscale systems have the potential to be used as diagnostic devices to detect diseases at preliminary stages, as well as discovery tools to find new clinically relevant biomarkers. But a major hurdle in developing these systems is picking out the molecules of interest from complex biological samples and concentrating them in one location for detection.

Now Kuo-Tang Liao and Chia-Fu Chou demonstrate an electrokinetic technique that can quickly concentrate traces of a protein at a single location (DOI: 10.1021/ja3016523). They created an array of nanoscale constrictions that work like molecular dams. The nanoconstrictions enhance the local electric field by 10^5-fold over the amount of applied field. Proteins, depending on their size and dielectric responses, get trapped at these nanoconstrictions.

To demonstrate their technique, Liao and Chou tested a fluorescently tagged streptavidin protein molecule and achieved a 10^5-fold enrichment in less than 20 s. The investigators say their approach is significantly faster than most other reported methods, and they suggest that their molecular dams may be particularly suitable in miniaturized devices designed for early disease diagnostics or general protein assays. **Rajendrani Mukhopadhyay, Ph.D.**

NEW STUDY REVEALS SYNTHETIC PRINCIPLES UNDERLYING ORGANIC SEMICONDUCTORS

Researchers led by John Reynolds report synthetic principles that can be used to strategically design π-conjugated polymers for applications in a wide range of semiconductor technologies (DOI: 10.1021/ja301898h).

Organic, π-conjugated semiconductors have been widely applied in recent years as thin-film transistors, as well as sensors and photovoltaic devices. When it comes to designing organic molecules for semiconductor applications, desired characteristics include ease of processing in solution, good charge-carrier mobility, a wide optical absorption profile, and long-term environmental stability. But depending on the desired application, some of these characteristics are more important than others. Hence, organic semiconductors designed for a specific application tend to not be effective enough for applications in other devices, limiting the material's broad usefulness.

The research team performed a comprehensive study to determine the interplay between the molecular structure and the performance of copolymers—made of alternating units of electron-rich and electron-deficient repeats—in both thin-film and photovoltaic devices. They found correlations between the charge transport ability of an organic semiconductor material and its repeat unit structure, molecular weight distribution, and

Published: June 12, 2012

dx.doi.org/10.1021/ja305430t | *J. Am. Chem. Soc.* 2012, 134, 10307−10308

JACS
JOURNAL OF THE AMERICAN CHEMICAL SOCIETY
Communication
pubs.acs.org/JACS

Nanoscale Molecular Traps and Dams for Ultrafast Protein Enrichment in High-Conductivity Buffers

Kuo-Tang Liao[†,‡] and Chia-Fu Chou*[,†,⊥,∥]

[†]Institute of Physics, [‡]Institute of Molecular Biology, [⊥]Genomics Research Center, and [∥]Research Center for Applied Sciences, Academia Sinica, Taipei 11529, Taiwan

Supporting Information

ABSTRACT: We report a new approach, *molecular dam*, to enhance mass transport for protein enrichment in nanofluidic channels by nanoscale electrodeless dielectrophoresis under physiological buffer conditions. Dielectric nanoconstrictions down to 30 nm embedded in nanofluidic devices serve as field-focusing lenses capable of magnifying the applied field to 10^5-fold when combined with a micro- to nanofluidic step interface. With this strong field and the associated field gradient at the nanoconstrictions, proteins are enriched by the molecular damming effect faster than the trapping effect, to $>10^5$-fold in 20 s, orders of magnitude faster than most reported methods. Our study opens further possibilities of using nanoscale molecular dams in miniaturized sensing platforms for rapid and sensitive protein analysis and biomarker discovery, with potential applications in precipitation studies and protein crystallization and possible extensions to small-molecules enrichment or screening.

Miniaturized biosensors and bioanalytical systems promise to revolutionize the field of health care and personalized medicine in light of sample reduction, speed, and sensitivity.[1] However, mass transport has generally been recognized as a major limiting factor in the sensitivity and performance of miniaturized sensor platforms, in that miniaturization leads to penalties on passive transport of biomolecules to the sensor surface due to increased diffusion length from the bulk liquid or in the direction of the fluidic channels.[2] Further, for low-abundance protein analysis, sample enrichment is often regarded as the first prerequisite for high-resolution analysis, since chemical amplification methods are not readily available for proteins. These factors pose major challenges for early or acute disease diagnostics and biomarker discovery using micro- or nanoscale sensor platforms. We report a new method for rapid enrichment and mass transport of proteins based on electrodeless dielectrophoresis (eDEP)[3] using an array of insulating nanoconstrictions as molecular *traps* or *dams* (preferred implementation), depending on the corresponding dielectric response of the molecules. We show that nanoconstrictions, serving as *field lenses*, may enhance local electric field to ~10^5-fold over the applied ac field and the associated field gradient. As a result of this strong field at the nanoconstrictions, Alexa-488-labeled streptavidins (52.8 kDa, 5 nm in diameter) are enriched by the molecular damming effect to $>10^5$-fold in <20 s in high-conductivity physiological buffers, orders of magnitude faster than most reported methods.[4] Our study opens further possibilities of using nanoscale molecular dams in miniaturized platforms for sensitive protein analysis, biomarker discovery, precipitation studies, and protein crystallization.[5]

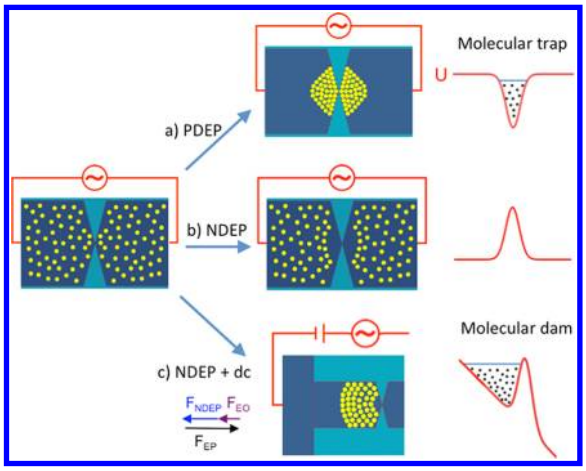

Figure 1. Concept of nanoscale molecular trap and dam. When an ac electric field is applied across an insulating nanoconstriction with a gap of tens of nm embedded in a sealed channel, the field can be highly focused, and a strong field gradient is generated for (a) *positive* dielectrophoresis (PDEP) or (b) *negative* dielectrophoresis (NDEP) if the dielectric permittivity of an analyte (shown in dots) is *larger* or *smaller* than that of the medium, respectively. The attractive potential in (a) serves as a *molecular trap*, while the repulsive potential in (b) keeps molecules away from the constriction. However, if a dc bias is applied in the case of NDEP, as shown in (c) for negatively charged particles, it tilts the repulsive potential into a slanted well, where the force balance condition, $F_{EP} = F_{EO} + F_{NDEP}$, occurs at local potential minimum, which could then cause protein accumulation in a continuous fashion, effectively working as a *molecular dam*.

Among the efforts for protein enrichment, electrokinetic methods using ion exclusion-enrichment effect by electrical double-layer (EDL) overlapping in a nanofluidic channel, or ion-selective permeable membranes such as Nafion, have been the most commonly adopted.[4a−h] Other methods based on conductivity gradient,[4j] temperature gradient,[4k−m] and patterned membranes[4n] for preconcentration have also been

Received: February 19, 2012
Published: May 17, 2012

dx.doi.org/10.1021/ja3016523 | J. Am. Chem. Soc. 2012, 134, 8742−8745

demonstrated. However, integrating sensing elements into these methods is not straightforward, since preconcentration is localized at the edges of the nanochannels. On the other hand, DEP[6] and the recently introduced eDEP,[3,7] or insulator-based dielectrophoresis (iDEP),[8] are known to be effective in the enrichment of DNA,[3,9] RNA,[10] viruses,[11] and cells[7,12] by exploiting the dielectric response of the bioparticles and its interaction with non-uniform electric fields. In particular, eDEP and its integration of DNA sensors demonstrated simultaneous sample enrichment and sensing.[13] However, recent reviews on eDEP cast doubts as to whether it could be implemented on chip for protein enrichment since either the size or the polarizability of proteins is much smaller than those of DNA or cells, and hence the demand for ultrahigh field gradient may not be easily realized.[14] In the current study, while we utilize highly focused fields at nanoconstrictions to enhance DEP forces, we alleviate problems associated with sensor integration by applying negative dielectrophoresis (NDEP) with dc bias; i.e., the net transport from electrophoresis (EP) is opposed by NDEP and electroosmosis (EO) through the force balance condition, $F_{EP} = F_{EO} + F_{NDEP}$, to enrich proteins away from the nanostructured points, a scheme we call a *molecular dam* (Figure 1). This scheme holds in general as long as the ac field imposes a strong NDEP scenario (ac field amplitude ≫ dc bias) at the constriction.

Classical DEP theory defines the translational force, i.e., the dielectrophoretic force, acting on a polarizable particle in a non-uniform field as $F_{DEP} = 2\pi r^3 \varepsilon_m Re[K(\omega)]\nabla E^2$, where r is the radius of the particle, ε_m the absolute permittivity of the suspending medium, E the amplitude of the applied field (i.e., root-mean-squared E in the case for an ac field), and $Re[K(\omega)]$ the real part of the Clausius−Mossotti (CM) factor, representing the frequency-dependent dielectric contrast between the particle and the suspending medium in an external driving field.[4h] It determines whether the particle transport is *toward*, when $Re[K(\omega)] > 0$, or *away from*, when $Re[K(\omega)] < 0$, the high field gradient region of the fluidic channel, correspondingly by *positive* dielectrophoresis (PDEP) or NDEP. The nanoscale molecular traps and dams implemented in this study are depicted in Figure 1.

Since F_{DEP} is proportional to the size of the molecules ($\sim r^3$), for proteins of few nanometers in size (~10—100 kDa) and small CM factor due to low polarizability, it is challenging within conventional devices to enrich proteins by DEP.[14] To overcome this issue, one needs to create a highly focused field and field gradient to enhance F_{DEP} by engineering the ∇E^2 (or $\mathbf{E}\cdot\nabla E$) term described above. The use of insulating nanoconstrictions provides both an enhanced field and field gradient to compensate the small size and low CM factor of the proteins, and to overcome its large diffusion coefficient. Based on this disposition, we have developed a fabrication process to construct eDEP nanoconstrictions embedded in nanofluidic channels (nanochannels) with interconnections to microfluidic channels for sample handling. (Device fabrication is detailed in the Supporting Information (SI).) To achieve nanoscale eDEP devices, fused silica was selected as the insulating substrate due to its robustness and low auto-fluorescence. The experimental layout and overall chip configuration are displayed in Figure 2a,b. Optical and scanning electron micrographs (Figure 2c,d) show that parallel nanochannels containing arrayed nanoconstriction structures may be constructed on one chip.

Due to the simple fact that the displacement current in a conducting buffer may be focused (or enhanced) by reducing of

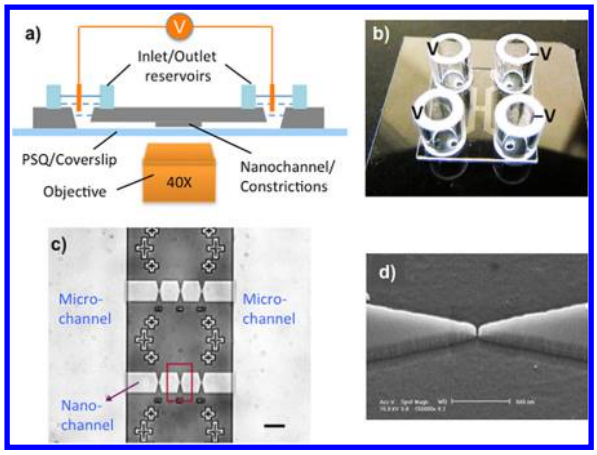

Figure 2. (a) Schematic of the experimental layout. Four Au electrodes are inserted into the reservoirs, shown in (b), where the electric field is applied. Experiments are monitored by an inverted fluorescence microscope via a 40× objective and an EMCCD (see Supporting Information). (b) Photograph of an assembled device (14×14 mm^2) made in fused silica (see Figure S1). The two reservoirs at each side of the H-shaped microchannel, 750 μm × 3 μm, are kept at equal potential. (c) Optical micrograph showing the center of the "H" where long nanofluidic channels (30 μm × 220 nm) are connected by microfluidic channels. Three nanoconstrictions are seeded in each of the five nanochannels (two shown here). (d) SEM image of the boxed nanoconstriction (viewed in 90° turn) in (c), with 30 nm gap size. Scale bar: (c) 30 μm; (d) 500 nm.

a cross-section of an insulating fluidic channel, it is straightforward to estimate the field-focusing factor in our device. If a microchannel with dimensions $X_{micro}\times Z_{micro}$ (width×height) is reduced to a nanochannel of $X_{nano}\times Z_{nano}$, and the nanochannel is further reduced to a nanoconstriction of width X_c, then from the continuity equation (current conservation) one can easily find the design rule for the overall field lens power to be $(X_{micro}/X_{nano})\times(Z_{micro}/Z_{nano})\times(X_{nano}/X_c)/n$, where n is the number of parallel nanochannels ($n = 5$ in our device), provided the conductivity of the buffer remains constant over all fluidic passages. This assumption is valid as the Debye screening length (<1 nm) in the buffers used in our experiments is much less than the nanoconstriction width and nanochannel height of our device. This condition is still far from the EDL overlapping scenario, where the concentration polarization effect is prounced.[4a−f] From our current design, the cross section of the microchannel is 750 μm × 3 μm^2, and that of the nanochannel is 30 μm × 220 nm, with nanoconstriction width 30 nm. The overall field-focusing factor is $\sim 7\times 10^4 X$, leading to an enhancement factor of $\sim 5\times 10^9$ for the dielectrophoretic force ($\sim E^2$) at the nanoconstrictions.[3,7] Empowered by such a strong enhancement of the field and field gradient, we were able to perform both PDEP and NDEP in our device using Alexa-488-labeled streptavidins as model proteins in physiological buffer conditions (10 mM phosphate-buffered saline with 150 mM NaCl, conductivity 1.6 S/m). Conversely, conventional metal electrode-based dielectrophoresis (MDEP) is not effective to overcome the strong EDL screening effect, due to the limitation of applied field strength, and hence could not easily polarize the protein−counterion cloud complex in high-salt conditions.[4a,c,h] On the other hand, the protein enrichment schemes using the co-ion depletion effect, caused by EDL overlapping, suffer from the relatively low

dx.doi.org/10.1021/ja3016523 | J. Am. Chem. Soc. 2012, 134, 8742−8745

potential barrier; hence, high dc bias cannot be applied for rapid protein accumulation.[4a−d,g,h]

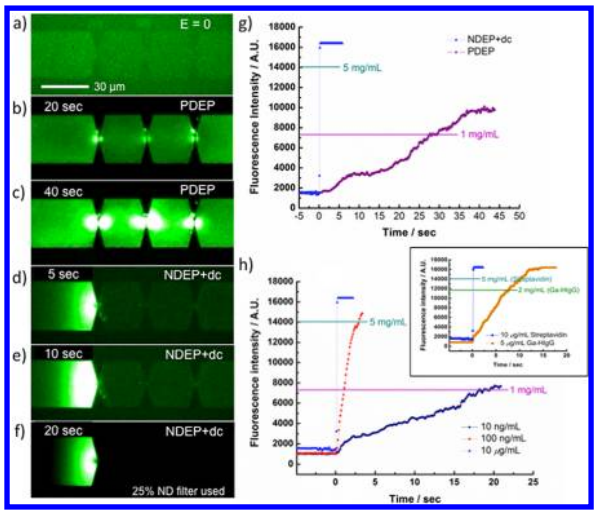

Figure 3. Protein trapping and damming with nanoscale eDEP. (a) Proteins (Alexa-488 streptavidins, 10 μg/mL) loaded in the chip by capillary force. Protein trapping with PDEP (b) 20 and (c) 40 s after 473 V_{pp}/cm ac field applied across the chip at 10 kHz. This field is focused 7×10^4-fold (~3.3×10^9 V_{pp}/m) over the applied field at the constrictions. All three constrictions show trapping of streptavidins, indicating PDEP is at work. (d−f) Protein damming demonstrated by NDEP+dc: ac field of 214 V_{pp}/cm is applied at 1 MHz with 1.5 V/cm dc bias (with positive potential at the right side of the channel). The image in (f) was taken with a 25% transmittance neutral density (ND) filter to keep the intensity below saturation of the EMCCD. The dark zone at the center of the first constriction indicates NDEP is at work where streptavidins are repelled. Virtually no excess molecules go beyond the first dam before reaching its saturation for effective accumulation at the second and third dams to show dark zones with good contrast. (g) Corresponding intensity plot of protein enrichment, at the same initial concentration of 10 μg/mL, under the same experimental conditions used for molecular trapping and damming. The plateau in the damming curve means the EMCCD has reached saturation (an extended intensity plot with the use of ND filter is shown in Figure S2). (h) Protein enrichment curves for various initial concentrations (10 ng/mL or 189 pM, 100 ng/mL, and 10 μg/mL) when operated under the molecular damming effect with corresponding dc bias of 1.5, 4.5, and 1.5 V/cm. The concentration rulers of streptavidin are drawn as horizontal lines. Note that 10 ng/mL proteins are enhanced >10^5-fold in <20 s. The inset shows the damming of goat anti-human IgG, which reaches 400-fold enrichment in 7.5 s from a concentration of 5 μg/mL (33 nM), against streptavidins (500-fold enrichment in <1 s) under the same applied field conditions as in (d−f).

Figure 3 summarizes our observation of the molecular trapping and damming effects through the operation of PDEP and NDEP with dc bias, respectively. Panels a−c demonstrate that PDEP for streptavidins may operate in arrayed nanoconstrictions and occurs at 10 kHz. However, when the frequency is increased to ~1 MHz, the DEP undergoes a crossover response from PDEP to NDEP with a changed sign of $K(\omega)$, consistent with other published results.[16] Panels d−f show the molecular damming effect for streptavidin enrichment when operated under NDEP with dc bias. These observations verify that the concepts depicted in Figure 1 are at work.

To compare the effectiveness of protein enrichment by PDEP (trapping) and NDEP with dc bias (damming), we loaded the chips with the same initial concentration of 10 μg/mL Alexa-488 streptavidins. Figure 3g indicates that the damming effect is much more efficient in protein enrichment, as 10^3-fold concentration enhancement may be achieved 2−3 s after the field is turned on, much faster than the trapping effect (see SI Figure S2 and Movies M1 and M2). In fact, this result suggests that, for practical applications, nanoscale eDEP as a molecular dam (NDEP+dc) is particularly advantageous for three reasons: it is much more effective in protein enrichment than PDEP; concerns of potential Joule heating effect are alleviated by displacement of the molecular dam away from the hot spot, i.e., the geometrical center of the nanoconstriction; and the sensing element can be placed micrometers away from the nanoconstriction, a task easily achievable by conventional photolithography. This circumvents the great technical challenge of integrating biosensors at the center or in the immediate proximity of the nanoconstrictions when operating in PDEP scheme.

To further characterize the enrichment factors for different initial protein concentrations under molecular damming conditions, streptavidins of 10 ng/mL, 100 ng/mL, and 10 μg/mL were loaded into the chips. Figure 3h shows the enrichment curves at various starting concentrations of streptavidin, where the concentration rulers of 1 and 5 mg/mL are drawn as horizontal lines under the same buffer conditions as those used in experiments to serve as references for calculating the enrichment factor and the time needed to reach the concentration rulers. To ensure the molecular damming strategy developed here is applicable to other proteins, we also tested Alexa-488-labeled goat anti-human IgG (~150 kDa, see SI) in comparison to Alexa-488 streptavidins (inset in Figure 3h). The results indicate the effect of the molecular size and the polarizability for different proteins. Note that all the data presented in Figure 3g,h and Figure S2 are plotted from the region of highest intensity of fluorescent signals (with an area of 9.6 μm^2 or 24 pixels) where proteins are mostly enriched, after subtracting the background from dark counts and auto-fluorescence from the substrate. Based on these results, a protein enrichment factor of >10^5-fold may be achieved in just seconds when operating in the damming scheme, orders of magnitude faster than most previous studies.[4a,c,h] We attribute the fast transport of molecules to the highly constricted field at both the micro- to nanochannel junction and the nanoconstriction. This is indeed a unique feature of our device. Streptavidin velocity is enhanced from ~1.5 μm/s in microchannel (1.5 V/cm applied dc bias and bulk mobility 0.8 ± 0.9 μm-cm/V-s)[4j] to ~100 μm/s by a 70-fold field enhancement when entering into the nanochannel, and further to ~10−15 cm/s by another 1000-fold field enhancement from the junction to the nanoconstriction (~45 μm distance). To estimate the effective potential energy U_{min} involved in the damming process using Boltzmann distribution, 10^5-fold concentration enrichment corresponds to $U_{min} \approx -12\ k_BT$, where k_BT is the thermal energy. Since in the experiments the system did not reach equilibrium as proteins kept accumulating during the process, this estimation would suggest a lower bound of the effective potential well.

To demonstrate that the balance of F_{EO} and F_{EP} alone cannot achieve the significant protein enrichment observed in our device, we studied the case of a pure dc field (up to 4.5 V/cm) but did not observe any discernible protein enrichment (see SI, Movie M3). In fact, it suggests F_{EP} is much higher than F_{EO} in our device. To further demonstrate the essential role of F_{NDEP}

dx.doi.org/10.1021/ja3016523 | J. Am. Chem. Soc. 2012, 134, 8742−8745

in molecular damming, we turned off the ac field but not the dc bias and observed the highly enriched proteins quickly diffusing away due to the concentration gradient established by the molecular dam (see SI, Movie M4). Hence, F_{NDEP} is essential for the protein damming effect in our design.

The potential Joule heating effect due to the highly focused field (total current 25 μA, or 5 μA/nanochannel) at the nanoconstrictions may be alleviated by the small sample volume (~1 pL/nanochannel), with a 220 nm liquid layer in the nanochannels, used in our devices. Hence heat dissipation through the substrate, as a bulk thermal bath, is very effective based on our previous study by finite-element multiphysics simulation.[13,17] Within our experimental conditions, we assume the proteins at the trap are not denatured, as the trapping events are reversible, and there is no denaturation-associated aggregation observed in our experiments. The issues discussed here are further assuaged if one operates the device as molecular dams where enriched proteins are away from the highly focused field constrictions.

Although protein trapping has been demonstrated using a 100-nm nanopipet with quasi-dc driving field,[18] and insulator post-array with dc field (iDEP with low-conductivity buffers to avoid Joule heating),[19] it remains challenging to detect ultra-low protein targets due to the limited protein enrichment factor achieved (up to 1000-fold) and to integrate it within a fluidic chip platform where multiplexing and parallel analysis are desirable (in the nanopipet approach). However, the concept of the molecular damming effect introduced in this study is exceedingly compatible with multiplexing, parallel analysis, and high-conductivity buffers, and thus suitable for integrating biosensors.

In summary, we present a nanoscale active molecular transport scheme for ultrafast protein enrichment by constructing nanoscale molecular traps and dams using electrodeless dielectrophoresis generated by insulating nano-constricted structures. A protein enrichment factor >10^5 has been achieved in <20 s, orders of magnitude faster than most of the reported methods. Multichannel layout for parallel operation has also been demonstrated. In this scenario, miniaturization alleviates rather than accentuates the transport limitations, so that any sensor applications can capitalize on the ultrafast sample enrichment schemes introduced here. Though our device could also be applied to DNA and RNA analysis,[3,10,13] it may find applications in general protein assays, protein crystallization, rare biomarker discovery (e.g., coupled with mass spectroscopy), and early disease diagnostics in lab-on-a-chip systems, with potential extensions to enrichment or screening of small molecules (e.g., peptides or carbohydrates).

■ ASSOCIATED CONTENT

Supporting Information

Details of device fabrication and protein enrichment; movies showing molecular trapping and damming effects. This material is available free of charge via the Internet at http://pubs.acs.org.

■ AUTHOR INFORMATION

Corresponding Author

cfchou@phys.sinica.edu.tw

Notes

The authors declare no competing financial interest.

■ ACKNOWLEDGMENTS

This work was supported by an AS Postdoctoral Fellowship (to KTL), AS Nano Program and Foresight Project (AS-97-FP-M02), NSC-Taiwan (99-2112-M-001-027-MY3), and USAF-AOARD (FA2386-12-1-4002). We thank Dr. Qi-Huo Wei for his early involvement of this project, Prof. N. S. Swami for critical comments on the manuscript, Drs. C. H. Lee and T. Leichle for helpful discussions, and AS Nano Core Facility.

■ REFERENCES

(1) (a) Vilkner, T.; Janasek, D.; Manz, A. *Anal. Chem.* **2004**, *76*, 3373. (b) Dittrich, P. S.; Manz, A. *Nat. Rev. Drug Discov.* **2006**, *5*, 210.

(2) (a) Nair, P. R.; Alam, M. A. *Appl. Phys. Lett.* **2006**, *88*, 233120. (b) Sparreboom, W.; van den Berg, A.; Eijkel, J. C. T. *Nat. Nanotech.* **2009**, *4*, 713. (c) Sheehan, P. E.; Whitman, L. J. *Nano Lett.* **2005**, *5*, 803. (d) Cohen, A. E.; Fields, A. P. *ACS Nano* **2011**, *5*, 5296.

(3) Chou, C.-F.; Tegenfeldt, J. O.; Bakajin, O.; Chan, S. S.; Cox, E. C.; Darnton, N.; Duke, T.; Austin, R. H. *Biophys. J.* **2002**, *83*, 2170.

(4) (a) Wang, Y.-C.; Stevens, A. L.; Han, J. *Anal. Chem.* **2005**, *77*, 4293. (b) Huang, H.; Xu, F.; Dai, Z.; Lin, B. *Electrophoresis* **2005**, *26*, 2254. (c) Kim, S. M.; Burns, M. A.; Hasselbrink, E. F. *Anal. Chem.* **2006**, *78*, 4779. (d) Armenta, J. M.; Gu, B.; Thulin, C. D.; Lee, M. L. *J. Chromatogr. A* **2007**, *1148*, 115. (e) Huang, K. D.; Yang, R. J. *Electrophoresis* **2008**, *29*, 4862. (f) Wu, D. P.; Steckl, A. J. *Lab Chip* **2009**, *9*, 1890. (g) Nie, F.-Q.; Macka, M.; Paull, B. *Lab Chip* **2007**, *7*, 1597. (h) Lee, J. H.; Song, Y.-A.; Han, J. *Lab Chip* **2008**, *8*, 596. (i) Greenlee, R. D.; Ivory, C. F. *Biotechnol. Prog.* **1998**, *14*, 300. (j) Inglis, D. W.; Goldys, E. M.; Calander, N. P. *Angew. Chem., Int. Ed.* **2011**, *50*, 7546. (k) Ross, D.; Locascio, L. E. *Anal. Chem.* **2002**, *74*, 2556. (l) Matsui, T.; Franzke, J.; Manz, A.; Janasek, D. *Electrophoresis* **2007**, *28*, 4606. (m) Ge, Z. W.; Wang, W.; Yang, C. *Lab Chip* **2011**, *11*, 1396. (n) Cheetham, M. R.; et al. *J. Am. Chem. Soc.* **2011**, *133*, 6521.

(5) Vilozny, B.; Actis, P.; Seger, R. A.; Pourmand, N. *ACS Nano* **2011**, *5*, 3191.

(6) Pethig, R. *Biomicrofluidics* **2010**, *4*, 022811.

(7) Chou, C.-F.; Zenhausern, F. *IEEE Eng. Med. Biol. Mag.* **2003**, *22*, 62.

(8) Cummings, E. B.; Singh, A. K. *Anal. Chem.* **2003**, *75*, 4724.

(9) Asbury, C. L.; van den Engh, G. *Biophys. J.* **1998**, *74*, 1024.

(10) Giraud, G.; et al. *Biomicrofluidics* **2011**, *5*, 024116.

(11) (a) Lapizco-Encinas, B. H.; Rito-Palomares, M. *Electrophoresis* **2007**, *28*, 4521. (b) Hughes, M. P.; Morgan, H.; Rixon, F. J.; Burt, J. P. H.; Pethig, R. *Biochim. Biophys. Acta* **1998**, *1425*, 119.

(12) (a) Pethig, R. *Crit. Rev. Biotechnol.* **1996**, *16*, 331. (b) Lapizco-Encinas, B. H.; Simmons, B. A.; Cummings, E. B.; Fintschenko, Y. *Anal. Chem.* **2004**, *76*, 1571.

(13) Swami, N.; Chou, C. F.; Ramamurthy, V.; Chaurey, V. *Lab Chip* **2009**, *9*, 3212.

(14) (a) Regtmeier, J.; Eichhorn, R.; Viefhues, M.; Bogunovic, L.; Anselmetti, D. *Electrophoresis* **2011**, *32*, 2253. (b) Srivastava, S. K.; Gencoglu, A.; Minerick, A. R. *Anal. Bioanal. Chem.* **2011**, *399*, 301.

(15) Pohl, H. A. *Dielectrophoresis: The Behavior of Neutral Matter in Nonuniform Electric Fields*; Cambridge University Press: Cambridge, 1978.

(16) (a) Gascoyne, P. R. C.; Vykoukal, J. *Electrophoresis* **2002**, *23*, 1973. (b) Hughes, M. P. *Electrophoresis* **2002**, *23*, 2569. (c) Basuray, S.; Chang, H.-C. *Phys. Rev. E* **2007**, *75*, 060501.

(17) Chaurey, V.; Polanco, C.; Chou, C. F.; Swami, N. S. *Biomicrofluidics* **2012**, *6*, 012806.

(18) Clarke, R. W.; White, S. S.; Zhou, D.; Ying, L.; Klenerman, D. *Angew. Chem., Int. Ed.* **2005**, *44*, 3747.

(19) Lapizco-Encinas, B. H.; Ozuna-Chacon, S.; Rito-Palomares, M. *J. Chromatogr. A* **2008**, *1206*, 45.

Kuo-Tang Liao[1,2]
Mikiyas Tsegaye[1]
Vasudha Chaurey[1]
Chia-Fu Chou[2]*
Nathan S. Swami[1]

[1]Electrical & Computer Engineering, University of Virginia, Charlottesville, VA, USA
[2]Institute of Physics, Academia Sinica, Taipei, Taiwan

Received December 24, 2011
Revised March 26, 2012
Accepted April 14, 2012

Research Article

Nano-constriction device for rapid protein preconcentration in physiological media through a balance of electrokinetic forces

We describe a methodology to steeply enhance streptavidin protein preconcentration within physiological media over that achieved by negative dielectrophoresis (NDEP) through utilizing a DC offset to the AC field at nanoscale constriction gap devices. Within devices containing approximately 50-nm constriction gaps, we find that the addition of a critical DC field offset (1.5 V/cm) to the NDEP condition (~200 V_{pp}/cm at 1 MHz) results in an exponentially enhanced extent of protein depletion across the device to cause a rapid and steeply rising degree of protein preconcentration. Under these conditions, an elliptical-shaped protein depletion zone that is extended along the device centerline axis forms instantaneously around the constrictions to result in protein preconcentration along the constriction sidewall direction. Through a potential energy diagram to describe the electrokinetic force balance across the device, we find that the potential energy barrier due to NDEP is gradually tilted upon addition of DC fields, to cause successively steeper potential wells along the sidewall direction for devices containing smaller constriction gaps. Hence, for approximately 50-nm constriction gaps at a critical DC field, the ensuing narrow and deep potential energy wells enable steep protein preconcentration, due to depletion over an exponentially enhanced extent across the device.

Keywords:
Dielectrophoresis / Electrokinetics / Nanoanalysis / Preconcentration / Proteins
DOI 10.1002/elps.201100707

1 Introduction

The challenge of sensing rare numbers of biomarker proteins against a background of high concentration of other matrix proteins within physiologically relevant media requires methodologies for selective preconcentration of the biomarker in the proximity of the sensor [1]. Conventional chemical methods based on antibody depletion are unable to achieve the necessary degree of preconcentration, since the biomarkers are present at 10^6–10^{12}-fold lower levels than the background proteins in blood [2]. Hence, there is great interest in applying electrokinetic methods, especially within nanofluidic devices [3], where the required degrees of preconcentration may be achieved due to the large volume reduction. While prior approaches have investigated preconcentration using ion exclusion-enrichment effects due to electrical double layer overlap at the micro-to-nanofluidic interface [4–6], the resulting protein preconcentration at 10^3–10^6-fold levels requires several tens of minutes to an hour, and this method cannot effectively separate target biomarker proteins against a background of similarly charged and sized proteins in samples of physiological fluids. Dielectrophoresis (DEP) enables highly selective trapping of bioparticles based on the characteristic frequency response of the dielectric permittivity of the bioparticle versus that of the medium [7, 8], and it has been extensively applied toward sorting of somewhat similar sized biological cells with differing dielectric frequency response [9]. However, its application to smaller sized biomarkers, such as nanoscale proteins and fragments of ss-DNA, requires methods to enhance the local field to offset the steep fall in DEP trapping forces with particle size [10, 11]. Recently, through the application of devices with 500-fold dielectric constrictions (500 to 1 μm) to enhance the field, we have demonstrated the trapping of 150-base ss-DNA in media of high conductivity to enable target DNA preconcentration and sensing through hybridization with immobilized capture probes [12–14]. However, given the smaller sizes of proteins, the direct trapping of proteins by DEP requires much higher fields.

Correspondence: Dr Nathan S. Swami, Electrical & Computer Engineering, University of Virginia, Charlottesville, VA, USA
E-mail: nswami@virginia.edu
Fax: +1-434 924 8818

Abbreviations: NDEP, negative dielectrophoresis; **PDEP**, positive dielectrophoresis

*Additional corresponding author: Professor Chia-Fu Chou
E-mail: cfchou@phys.sinica.edu.tw

Colour Online: See article online to view Figs. 1–7 in colour.

Hence, higher voltages are needed for trapping within an electrode device format [15,16], which can affect protein functionality, and within electrode-less configurations, it requires nano-sized structures, such as proof-of-concept devices utilizing nano-pipettes [17] or nanotubes tips [18], which are not scalable. Other trapping methods within droplets [19], pose limitations on the media for protein preconcentration. Alternatively, indirect means can be applied to manipulate proteins through streaming DEP [20,21], to influence the net flow profiles in a microfluidic device, but the degree of control of protein trapping to enable preconcentration and separation is limited by the small magnitude of dielectrophoretic forces over other forces. Hence, optimizing the dielectrophoretic trapping of proteins within a scalable nanofluidic device is of interest, to assess the influence of device structure (surface charge at constriction tip and local electric field), electrical conditions (AC bias frequency and DC bias), and fluidic conditions (media conductivity and pH) on protein preconcentration and separation.

The trapping of proteins at room temperature conditions, within physiological media of neutral pH and high conductivity is necessary to maintain the conformation and biofunctionality of the protein. However, DEP trapping of proteins within media of high conductivity poses distinct challenges. First, the frequency response of the protein species in conducting media is difficult to interpret given the complex interplay of surface charges, mobile charges, and water molecules under the electric field, especially since counterion fluctuations influence the relaxation time for polarization of biomolecules [22, 23]. Second, the enhanced current flow due to localized fields within media of high conductivity (>1 S/m) causes Joule heating [24, 25], which can denature the proteins. Finally, while this problem can be overcome by applying negative DEP to trap proteins away from the high-field region, the resulting temperature gradients due to Joule heating can cause bulk electrothermal flow that can lower DEP preconcentration [13]. Hence, in order to enhance the degree of preconcentration, there is a need of methods to localize protein trapping under negative DEP (NDEP). Herein, through the application of a scalable nanofluidic device platform, we investigate the influence of DC bias coupled to the AC field on devices of successively smaller constriction gaps, to enable narrowing of the protein preconcentration band through a balance of electrophoresis, electro-osmosis, and NDEP forces. We find that steeply rising levels of protein preconcentration can be obtained only under conditions that enable a depletion zone of enhanced extent, which occurs almost instantaneously in proximity of approximately 50 nm constriction gaps, at frequencies characteristic of NDEP (1 MHz), and in presence of a critical DC bias (~1.5 V/cm). Using a potential energy diagram to describe the electrokinetic force balance across the device, we find that application of approximately 50 nm constrictions to enable a significant energy barrier to protein transport, in conjunction to a critical DC field to cause significant tilting of the energy profile results in the formation of narrow and deep potential wells for rapid protein preconcentration, due to protein depletion over an exponentially enhanced extent versus devices under subcritical DC or with larger constrictions.

2 Materials and methods

2.1 Nanoconstriction device

The fabrication of nanofluidic devices with nanoconstrictions for ultrafast protein preconcentration is based on our previously developed insulator constriction-based dielecrophoresis device (see Supporting Information) [26]. A microfluidic channel was constructed by photolithography on a fused-silica substrate, of 3 μm depth and 750 μm width, with outer constrictions to form five "nanochannels" of 200 nm depth and 30 μm width. Following this, electron beam lithography was applied to nanofabricate multiple inner constrictions within the nanochannel of varying sizes (15 nm to 150 nm), as confirmed by scanning electron microscopy. The whole device, with integrated micro (3 μm depth) and nanofluidic (200 nm depth) channels was completed at room temperature using a low-pressure sealing process [27]. The final nanofluidic device is shown in Fig. S1 of the Supporting Information.

2.2 Protein preconcentration and imaging

This device was subsequently applied toward rapid protein trapping under positive DEP (PDEP) at approximately 200 V_{pp} across approximately 1 cm at 100 kHz, and negative DEP (NDEP) at approximately 200 V_{pp} across approximately 1 cm at 1 MHz, using an Agilent function generator (33220A) and an FLC voltage amplifier (A400D). To enhance preconcentration under NDEP, we investigated additional DC offsets of approximately 0.3 V/cm and approximately 1.5 V/cm field strength. The preconcentration of fluorescently labeled streptavidin protein samples (52.8 kDa, Molecular Probes, Engene, OR, USA), at μg–ng/mL concentration levels, within an electrolyte of 10 mM PBS containing 150 mM NaCl and 2 mM NaN_3, at pH 7.2, was imaged using an inverted Zeiss Observer microscope with a Hammatsu EM-CCD to enhance sensitivity.

2.3 Modeling methods

The electric potential within the nanofluidic device can be mapped through solving the Laplace equation to determine the equipotential lines:

$$\nabla \cdot ((\sigma + j\omega\varepsilon)\nabla\phi) = 0 \quad (1)$$

The electric field distribution can then be obtained using the relation:

$$\vec{\mathrm{E}} = -\nabla\phi \tag{2}$$

Based on the electric field distribution in the device, its gradient can be calculated, which in turn can be used to determine the dielectrophoretic force profile across the device. At steady state, the average dielectrophoretic force, F_{DEP}, on a homogeneous spherical particle with electrical permittivity, ε_p, conductivity, σ_p, and radius, a, suspended in a fluid with electrical permittivity, ε_m, and conductivity, σ_m, in a nonuniform AC electric field, **E**, is given by the following in 3D with α, representing the polarizability:

$$\vec{\mathbf{F}}_{DEP} = 2\pi a^3 \varepsilon_m \mathrm{Re}\underbrace{\left(\frac{\varepsilon_p^* - \varepsilon_m^*}{\varepsilon_p^* + 2\varepsilon_m^*}\right)}_{K_{CM}} \nabla \vec{E}^2 = \alpha E.\nabla E \tag{3}$$

Here, $\alpha = 2\pi\varepsilon_m a^3 \left(\frac{\varepsilon_p^* - \varepsilon_m^*}{\varepsilon_p^* + 2\varepsilon_m^*}\right)$ and K_{CM} is the Clausius–Mossotti factor, which depends on the frequency (ω) of the applied field as given by: $\varepsilon^* = \varepsilon + \sigma/j\omega$. Since the DEP force is experienced by the polarized particles, only in nonuniform electric fields, it is proportional to the gradient (or spatial nonuniformity) of the square of the electric field. The electrophoresis force (F_{EP}) can be calculated from the electrophoretic mobility (μ_{EP}), using friction coefficient ($\gamma = 6\pi\eta a$; for protein particles of size, a, and medium viscosity: η) as:

$$\mathrm{F_{EP}} = \gamma\mu_{EP}\mathrm{E} \tag{4}$$

Similarly, the electro-osmosis force (F_{EO}) can be calculated from the electro-osmotic mobility (μ_{EP}) within the device and friction coefficient (γ):

$$\mathrm{F_{EO}} = \gamma\mu_{EO}\mathrm{E} \tag{5}$$

As in Fig. 1, under NDEP conditions, F_{NDEP} and F_{EO} oppose F_{EP} on the side of the constriction facing the inlet, as given by net force (F_{net}):

$$\mathrm{F_{net}} = \mathrm{F_{EP}} - \mathrm{F_{EO}} - \mathrm{F_{NDEP}} \tag{6}$$

On the side of the constriction facing the outlet, where no protein trapping occurs, F_{NDEP} and F_{EP} oppose F_{EO}, thereby reversing the sign on F_{NDEP} in Eq. (6). Since all steady-state electrical forces are conservative vector fields, we can calculate scalar potential energy fields, to describe the net electrokinetic force balance in terms of barriers and wells that affect particle trapping within the device. The potential field is given by the integral over the volume (dV) of the net electrokinetic force (F_{net}):

$$U = \oint F_{net}.dV \tag{7}$$

Based on Eqs. (3–6), this can be written as:

$$U = \oint_V \alpha \vec{E}\nabla\vec{E}dV + \oint_V \gamma(\mu_{ep} + \mu_{eo}) \cdot \vec{E}dV \tag{8}$$

This can be integrated to the following, based on the integral forms of Eq. (2) for the DC voltage, ΦDC:

$$U = \frac{\alpha\vec{E}^2}{2} - \gamma(\mu_{ep} + \mu_{eo}) \cdot \Phi_{DC} \tag{9}$$

3 Results

3.1 Device methodology for protein preconcentration

The methodology for the application of nanoscale constrictions to enable protein preconcentration through a balance of electrokinetic forces is schematically described in Fig. 1. Under NDEP conditions (~200 V_{pp}/cm at 1 MHz), protein molecules are pushed away from the constriction edge by F_{NDEP}, as shown in Fig. 1A. Within physiological media (~150 mM salt at pH 7.2) of high conductivity (σ_m ~1.6 S/m), the enhanced current and field cause a substantial level of Joule heating (see Supporting Information Fig. S3), with the resulting temperature gradients causing a net electrothermal flow. Based on prior work [28], the direction of electrothermal flow (F_{ETH}) is given by $-\nabla T{\cdot}E$. Within constriction DEP devices, since the temperature gradient (∇**T**) and the electric field (E) vectors are pointed toward the constriction edge [13], F_{ETH} is pointed away from the constriction edge, similar to the direction of F_{NDEP}. However, F_{NDEP} is highly localized at the constriction due to its dependence on ∇E^2, whereas F_{ETH} is more long ranged [24, 25], since it depends on E^2 and acts indirectly upon the particles through a drag force. Hence, under NDEP conditions within media of high conductivity, the protein trapping is spread over a diffuse region, thereby requiring a DC field to enable the observation of protein preconcentration. Upon the application of a small DC field in addition to the higher AC bias at 1 MHz, we enable the action of electrophoretic forces (F_{EP}) on the streptavidin protein particles, as well as electro-osmotic drag forces (F_{EO}) from the fluid, in conjunction to the NDEP forces. As shown in Fig. 1B, under electrophoresis, the negatively charged protein molecules (negative 2.3e, as per [3] for an elementary charge of "e") are drawn away from the terminal at negative potential (henceforth called "inlet"), toward the nanoconstriction. On the other hand, under electro-osmosis and negative DEP forces, the molecules are pushed away from the nanoconstriction and back toward the inlet. In the vicinity of the 1000–5000-fold constrictions used within this work, F_{NDEP} is substantially larger than F_{EP} and F_{EO}. Since protein preconcentration and depletion only occur on the side of the constriction facing the inlet, we assume that μ_{EP} exceeds μ_{EO}

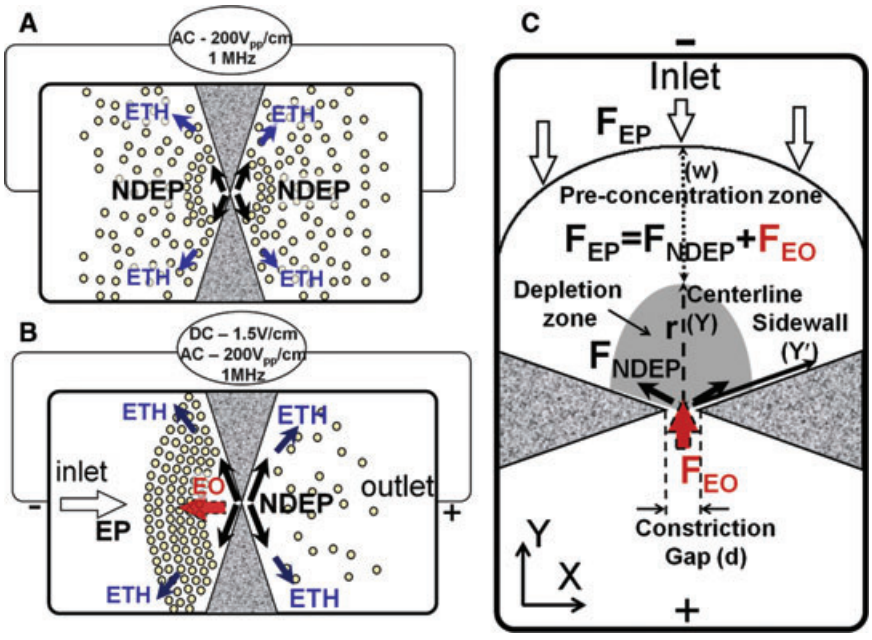

Figure 1. Schematics of protein preconcentration through an electrokinetic force balance: (A) Trapping under NDEP (NDEP) using AC bias only; (B) Applying an additional DC offset over the AC bias can localize protein preconcentration between the inlet and the constriction, as shown in (C) through a balance of electro-osmosis (F_{EO}) and NDEP (F_{NDEP}) versus electrophoresis (F_{EP}) to cause formation of the "depletion zone" of arc radius, *r*, near the constriction (grey), and the "preconcentration zone" of width *w*. The effect of constriction size (*d*) and applied field conditions (DC versus AC field) on protein preconcentration is studied by investigating the force balance along the centerline (*Y*) and sidewall vectors (*Y'*).

at all points across the device, so that in the proximity of the constriction where F_{NDEP} is substantial, the sum of electro-osmosis and NDEP forces can just equal the opposing electrophoresis force, as given by: $F_{EP} = F_{EO} + F_{NDEP}$. This would explain protein preconcentration onwards from this force balance point, with protein depletion occurring in the vicinity of the constriction, as in Fig. 1C. This assumption of $\mu_{EP} > \mu_{EO}$ also explains the absence of protein depletion and preconcentration on the side of the constriction facing the outlet where F_{NDEP} opposes F_{EO}. Hence, the force balance condition of: $F_{EP} + F_{NDEP} = F_{EO}$ will not be reached, given that $F_{EP} > F_{EO}$, and the addition of F_{NDEP} to F_{EP} would continue to be greater than F_{EO}. The high-salt levels within the medium (~150 mM salt) serve to enhance μ_{EP} over μ_{EO}, since the thinner electrical double layer around the channel wall reduces μ_{EO} and the smaller counter-ion cloud around protein molecules reduces retardation forces to electrophoresis arising from hydrodynamic drag and ion flow within the counter-ion cloud [29]. We have assumed μ_{EP} of approximately 1 μm.cm.V^{-1}s^{-1} [3]; and approximately 10-fold lower μ_{EO}, with the DEP mobility making up the difference in proximity of the constriction, as computed from an NDEP force using a Clausius–Mossotti factor (K_{CM}) of −0.5. These depletion and preconcentration zones occur along an arc, as in Fig. 1C. In this manner, the trapping region can be narrowed to enhance the degree of protein preconcentration in comparison to what can be achieved using NDEP only. The degree of protein preconcentration can be further enhanced by the development of conditions to enhance the extent of the depletion zone (*r*) or reduce the width of the preconcentration zone (*w*). In the following sections, we investigate the critical values of the DC field, AC frequency, and constriction size (*d*) required to cause rapid enhancement of protein preconcentration through exploring the profile of the electrokinetic force balance (F_{net}, in Eq. (6) across the device. Specifically, we compare the force balance along directions of the centerline (vector **Y** along device length) and sidewall (vector **Y'** along constriction edge), as in Fig. 1C, to track formation of the depletion and preconcentration zones.

To optimize the electrokinetic force balance for enhanced protein preconcentration, the time evolution of protein preconcentration was investigated at devices of varying nanoconstriction gap size (30 μm channel constricted to *d* ~50 nm, ~100 nm or ~140 nm) and under varying DC field offsets (~0.3 V/cm or ~1.5 V/cm) over the AC field conditions for NDEP. Figure 2 shows time-lapse fluorescence images for protein trapping in the region close to the device constriction under NDEP conditions (~200 V_{pp}/cm AC field at 1 MHz) with an added DC field (~1.5 V/cm) for devices with constrictions of approximately 50 nm (Fig. 2A–C) versus approximately 140 nm (Fig. 2D–F). At both constriction sizes, a dark circular arc corresponding to depletion of the fluorescently labeled proteins (henceforth called the depletion zone) on the concave edge of the arc toward the constriction is apparent within a fraction of a second after the field is turned on. On the convex edge of the arc away from the constriction, we notice a strong degree of preconcentration of the fluorescently labeled proteins (henceforth called the preconcentration zone), especially close to the sidewall direction. It is noteworthy that at both constriction sizes, the depletion zone is established almost instantaneously and does not significantly evolve over time, while the preconcentration zone evolves over time. The constriction gap size on the device strongly affects the shape of the arc and its extent from the constriction (*r*). For larger constrictions (*d*~140 nm), the arc forms as a semicircle, whereas for smaller constrictions (~50 nm), the arc is

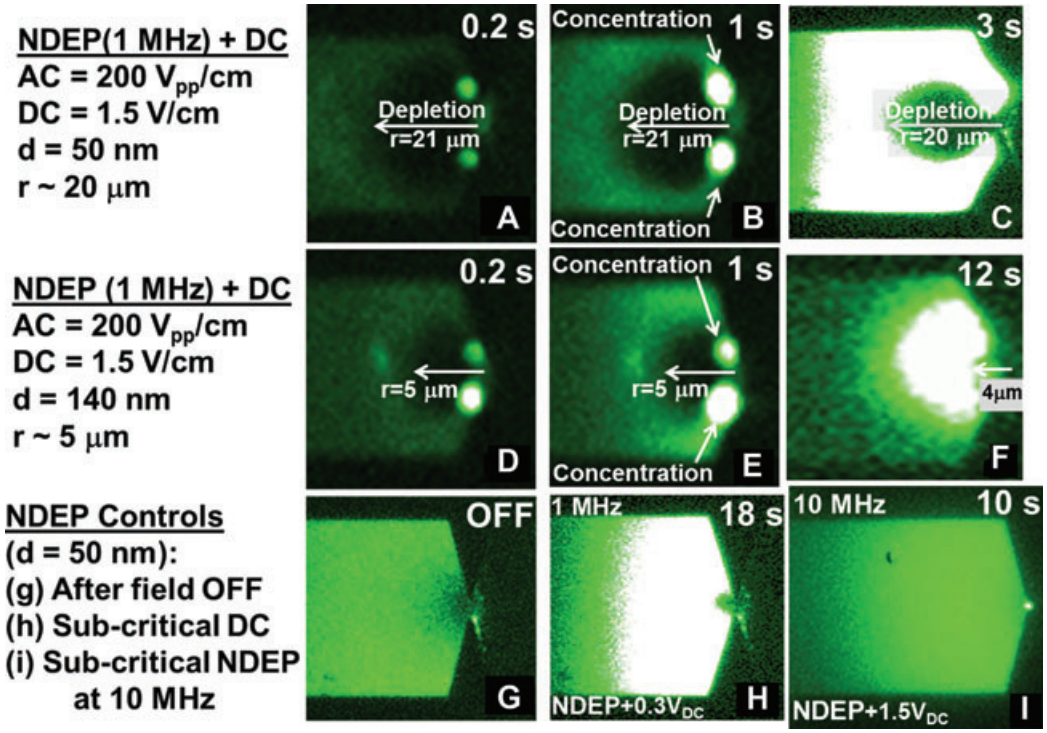

Figure 2. Time evolution of protein preconcentration at nanoconstriction devices of varying size (d = 50 versus 140 nm) and DC offset of 0.3 versus 1.5 V/cm to the NDEP field conditions (200 V_{pp}/cm, 1 MHz). (A)–(C) fluorescence images of 50 nm constriction devices under 1.5 V/cm DC offset to NDEP show the instantaneous formation of the depletion zone (~20 μm) away from the device centerline and rapid emergence of the concentration zone close to the sidewall vector. (D)–(F) images of 140 nm constriction devices under 1.5 V/cm DC offset to NDEP show the instantaneous formation of a smaller depletion zone (~4 μm) away from the device centerline and gradual emergence of the concentration zone close to the sidewall vector.(G) Shows that the preconcentrated protein is immediately dispersed upon turning OFF the fields. (H) Shows that a subcritical DC offset of 0.3 V/cm is unable to form a large depletion zone (r <1 μm). (I) Shows that the lower NDEP force at AC frequencies of approximately 10 MHz, prevent formation of the depletion zone.

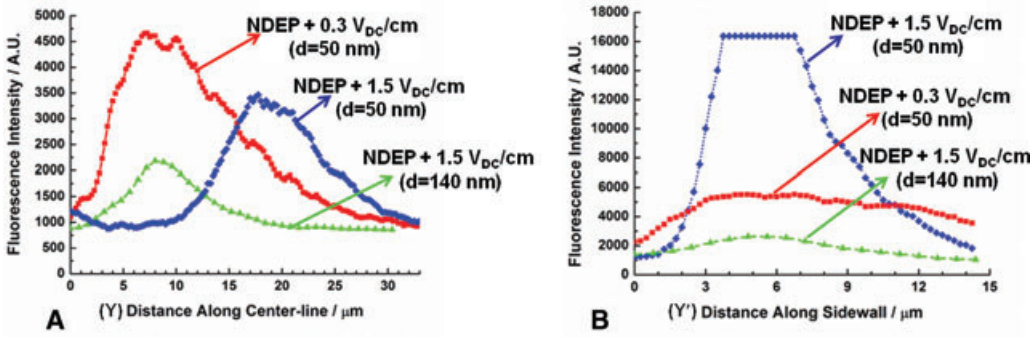

Figure 3. Line scan fluorescence intensity plots under NDEP conditions with additional DC bias (~0.3 V/cm or ~1.5 V/cm) and varying constriction size (~50 nm or ~140 nm) along: (A) the centerline vector (Y); (B) the sidewall vector (Y′).

extended along the length (Y-axis) versus the width (X-axis) of the channel. The extent of the arc (*r*), measured along the device centerline (Y) was exponentially enhanced from approximately 3–4 μm for approximately 140 nm constriction gaps to approximately 8–10 μm for 100 nm constriction gaps and approximately 20–22 μm for approximately 50 nm constriction gap devices, as shown in Fig. S4 of Supporting Information. At early time points, protein preconcentration is most significant along the sidewall direction (Y′ in Fig. 1C) and over time it extends cover rest of the convex edge of the arc facing the inlet, with an almost unchanging depletion region on the concave edge of the arc facing the constriction. From Fig. 2G, it is apparent that upon removal of the field, the preconcentrated protein molecules are completely dispersed across the device, demonstrating a completely reversible preconcentration process, without any discernible aggregation. At a subcritical DC field offset of 0.3 V/cm to the AC field under NDEP conditions (~200 V_{pp}/cm at 1 MHz), as shown in Fig. 2H, the depletion

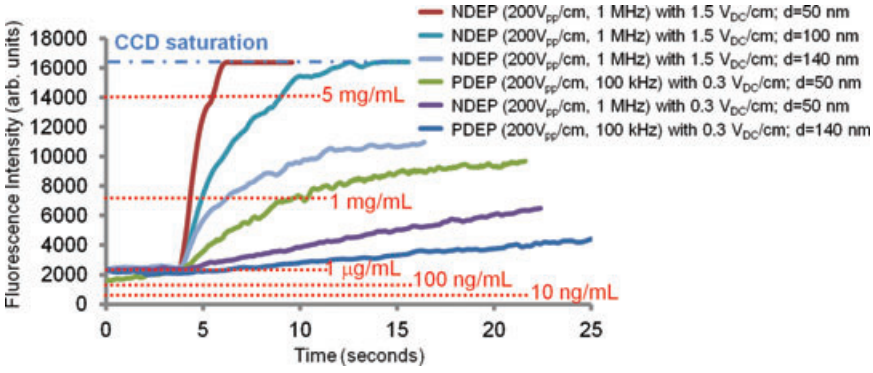

Figure 4. Time evolution of the fluorescence intensity plots show that an exponential level of protein preconcentration can be achieved *only* at devices with approximately 50 nm constriction gaps under NDEP conditions with a critical DC offset of 1.5 V/cm. Legends from top to bottom correspond to curves from left to right. The respective concentration levels for the respective fluorescence intensities as per the calibration curve are indicated.

zone has a very small extent (<1 µm) and the preconcentration zone is wide. Furthermore, significant depletion and preconcentration zones are not observed under AC frequency conditions that result in subcritical NDEP, such as at 10 MHz in Fig. 2I or in the approximately 30–300 kHz range, where only PDEP is apparent (Fig. S2, Supporting Information). Line scans of the fluorescence intensity plots along the centerline and sidewall vectors, in Fig. 3A and B, respectively, show that for devices with approximately 50 nm constriction gaps under NDEP conditions with approximately 1.5 V/cm DC field, the depletion zone is far more extended along the centerline versus the sidewall vector, with a far higher degree of protein preconcentration along the sidewall vector. On the other hand, for the same device under NDEP conditions plus subcritical DC (~0.3 V/cm), the preconcentration is uniform across the force balance arc, regardless of the centerline or sidewall direction. At larger constrictions (~140 nm), preconcentration is uniform across the arc, under NDEP conditions plus 1.5 V/cm DC field. In summary, the results show an exponentially enhanced extent of protein depletion (*r*) upon addition of a critical DC field to the NDEP conditions (Fig. S4, Supporting Information), especially at smaller constriction gaps.

Figure 4 shows the degree of protein preconcentration within devices of varying constriction sizes (~50, 100, or 140 nm), AC frequency (100 kHz for PDEP and 1 MHz for NDEP), and additional DC field offsets of approximately 0.3 or approximately 1.5 V/cm. The results are plotted as maximum fluorescence intensity (localized on the convex edge of the arc in proximity to the constriction tip) versus trapping time. The approximate local concentration level at critical fluorescence intensity levels as per the concentration calibration curve is indicated for reference. From this figure, it is clear that under NDEP conditions with subcritical DC field (~0.3 V/cm), the degree of protein preconcentration is not substantial, even for devices with approximately 50 nm constriction gaps. However, the addition of approximately 1.5 V/cm DC field to the NDEP conditions causes a rapid rise in the degree of protein preconcentration, far above what is obtained

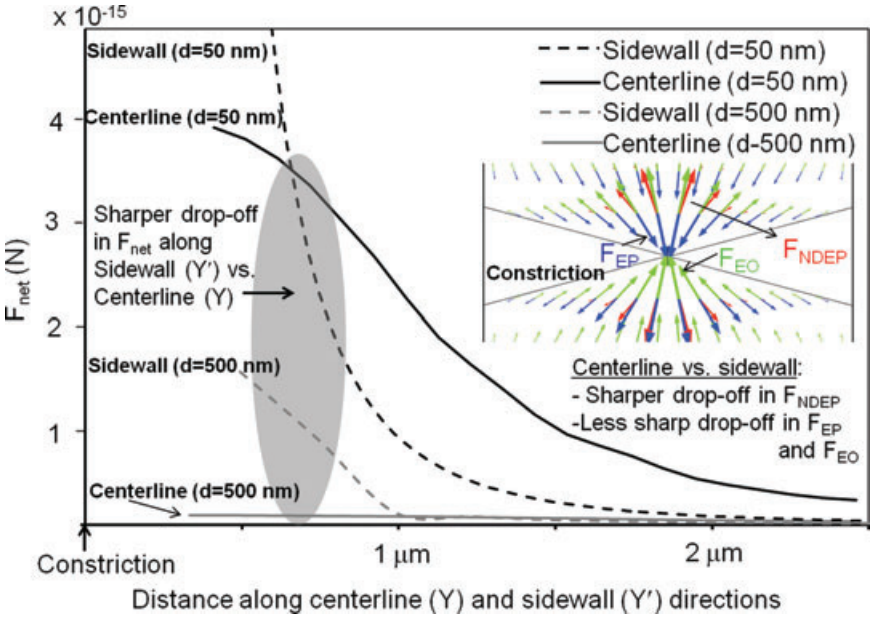

Figure 5. Simulations of the net force ($F_{net} = F_{DEP} - F_{EP} + F_{EO}$) along the centerline (*Y*) and sidewall (*Y′*) vectors (as per Figure 1C) show a sharp drop-off in the force along the sidewall versus the centerline vector. The inset shows the profile across the device of the electrophoresis (blue arrow) versus NDEP (red) and electro-osmosis (green) forces.

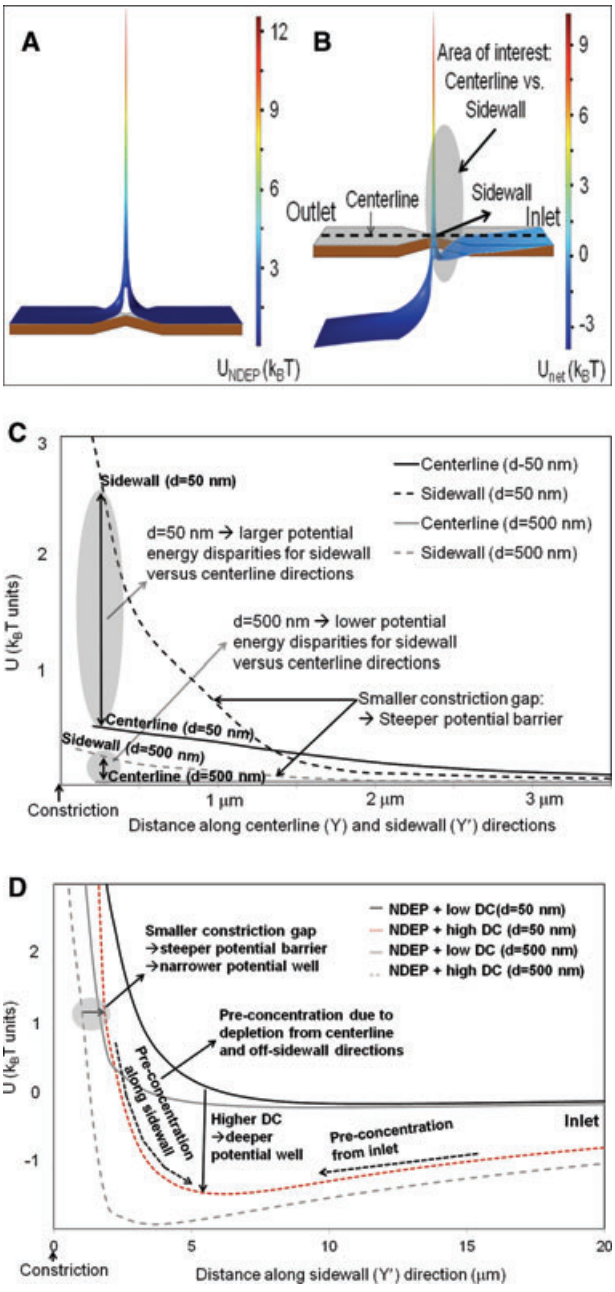

Figure 6. Simulation of potential energy profiles to explain formation of the depletion and preconcentration zones. (A) Under NDEP conditions (200 V_{pp}/cm, 1 MHz) at 50 nm constriction gap devices, a barrier of substantially high potential energy can be formed. (B) Upon the addition of a DC offset of 1.5 V/cm to the NDEP conditions, the barrier is tilted toward the inlet to form potential energy wells for protein preconcentration. (C) The sharp drop-off in potential energy away from the constriction along the sidewall versus the centerline vector is especially apparent within devices of smaller (~50 nm) versus larger (~500 nm) constriction gaps. (D) Under a critical DC offset under NDEP conditions, the potential profile is tilted to cause deeper and narrower wells for protein preconcentration.

under PDEP conditions inside the constriction region. The rise in degree of preconcentration is steep for 50 nm constriction devices, where the detector is saturated within 2 s, based on multiple data points acquired at 30 frames per second. In summary, these results indicate the enhanced extent of the protein depletion zone under conditions of a characteristic AC field (200 V_{pp}/cm at 1 MHz) and a critical DC offset of approximately 1.5 V/cm (as in Fig. 2) on devices with approximately 50-nm constriction gaps, can be directly correlated to rapid protein preconcentration (Fig. 4).

4 Discussion

The instantaneous formation of the protein depletion zone of enhanced extent (~20 μm) in the vicinity of the constriction of the approximately 50-nm gap devices and its direct correlation to the steeply rising degree of protein preconcentration is qualitatively explained in this section through applying device-level simulations to describe the electrokinetic force balance. In comparison, the depletion region reported within prior work [4–6] due to concentration polarization or electrical double layer overlap at the micro-to-nanofluidic interface evolves over time and hence, results in a slower degree of preconcentration. Furthermore, we seek to explain the disparities in protein preconcentration along the sidewall versus centerline directions that are observed only within the smaller constriction devices (~50 nm gap) under NDEP conditions (200 V_{pp}/cm, 1 MHz) with a critical DC field (1.5 V_{DC}/cm), as in Fig. 3. Finally, it is of interest to correlate these preconcentration disparities to the unexpectedly enhanced extent of the depletion zone (~20 μm in Fig. 2A–C) within these devices, given that the influence of the NDEP force should drop off within an extent (*r*) of approximately 1 μm away from the constriction edge and the total extent of the constriction gradient along the centerline vector is no more than 5 μm.

The inset of Fig. 5 shows a simulation of the direction and magnitude (length of the arrows) of the electrophoresis (blue), DEP (red), and electro-osmosis (green) forces across the device. It is readily apparent that similar to the schematic analysis presented in Fig. 1C, the electrophoresis and electro-osmosis forces oppose each other at all points within the device, and both of these forces rise continuously with the electric field due to gradient neighboring the constriction, to reach a maximum value at the constriction tip. F_{EP} exceeds the F_{EO} at all points within the device, with F_{NDEP} making up the difference in the region proximal to the constriction to cause preconcentration on the side facing the inlet as per the force balance condition: $F_{EP} = F_{NDEP} + F_{EO}$. Hence, in the absence of a critical level of F_{NDEP}, no significant protein preconcentration would occur, as apparent from the experimental results in Fig. 2I, where the preconcentration zone is insignificant under NDEP conditions at 10 MHz, due to lower F_{NDEP} in comparison to that at 1 MHz. Furthermore, while F_{EP} and F_{EO} scale with the field, F_{NDEP} scales as ∇E^2. Hence, based on field simulations, F_{NDEP} rises more sharply in the vicinity of the 50-nm constriction gap to a far higher

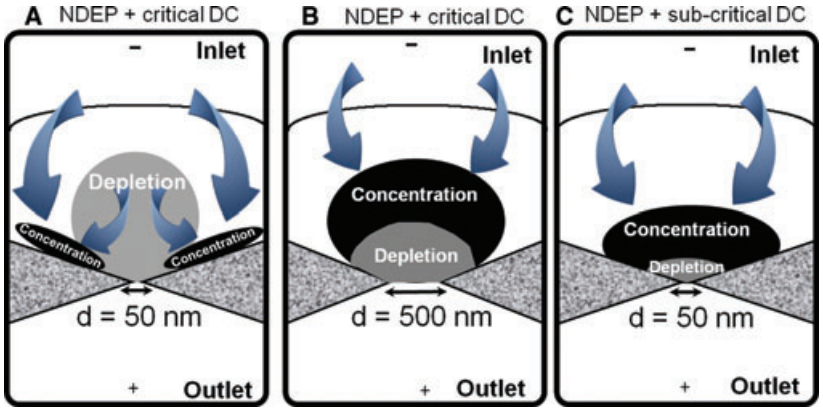

Figure 7. Schematics for formation of depletion and preconcentration zones: (A) NDEP conditions with a critical DC field offset at 50 nm constriction gaps causes large depletion zones and more localized preconcentration zones due to the large potential energy disparities along centerline versus sidewall direction. The respective potential energy disparities are relatively lower within devices of: (B) larger constriction gaps, due to broader potential wells; and (C) under conditions of subcritical DC, due to shallower potential wells, thereby causing depletions zones of lower extent and less localized preconcentration zones.

value (maximum of $\sim 10^{-11}$ N) than either F_{EP} (maximum of $\sim 10^{-12}$ N) or F_{EO} (maximum of $\sim 10^{-13}$ N), but F_{NDEP} also drops off more sharply away from the constriction tip. To better understand the effect of this on the electrokinetic force balance across the device, the net electrokinetic force (F_{net}, as in Eq. (6) is plotted in Fig 5., along the centerline versus sidewall directions for large (~500 nm) and small (~50 nm) constriction gaps. Approaching from the inlet (right side of the plot) toward the constriction (left side of the plot), the F_{net} rises more sharply along the sidewall versus the centerline direction due to the gradient resulting from the constriction, and this rise is sharper for the smaller constriction gap sizes. Based on the length of the arrows within the inset of Fig. 5, representing magnitude of the respective forces, it is clear that at an extent of *r* approximately 1 μm from the constriction, while F_{NDEP} almost equals F_{EP} along the centerline direction; it is insignificant in comparison F_{EP} along the sidewall direction. Hence, approximately 1 μm away from the constriction, the steeper drop in F_{net} along the sidewall versus centerline direction is directly attributable to the sharper drop off in F_{NDEP} along the sidewall versus centerline direction.

Next, we relate these force profiles to the scalar potential energy across the device to understand and optimize device designs for enhanced preconcentration, similar to prior work utilizing this methodology [30]. Specifically, we focus on applying this approach to qualitatively understand the shape and extent of the depletion region, as well as the location of preconcentration regions within the device. In Fig. 6A and B, the potential energy profile due to only F_{NDEP} (U_{DEP}) and F_{net} (U) is plotted in K_BT units, across from the entire device, from the inlet to the constriction to the outlet. Under AC field conditions (only NDEP), a potential energy barrier due to F_{NDEP} develops in close proximity of the constriction, which prevents protein particles from passing through the constriction. Upon addition of a critical level of DC field offset, the potential energy profile is tilted to result in "wells" for more localized protein trapping. The influence of the resulting wells across the centerline and sidewall directions is explored for devices of varying constriction gap size and DC bias in Fig. 6C and D. As the constriction is approached onward from the inlet, disparities emerge in the potential energy barrier along the sidewall versus centerline directions in Fig. 6C. These disparities are enhanced at smaller constriction gap size due to the substantially higher F_{NDEP} within smaller gaps, which manifests as a higher F_{net} or negative slope of the potential energy profile along the sidewall direction. Figure 6D shows that a greater DC field offset to tilt the potential energy profile can cause deeper potential wells for protein preconcentration from the inlet, as well as from regions of higher energy across the entire device, including those points along the centerline direction that have shallower and wider potential wells (due to smaller changes in F_{net} along the centerline versus sidewall direction, as per Fig. 5). Hence, within devices of smaller constriction gaps, at a critical DC field offset, the sidewall direction of the device has deepest and narrowest potential wells. This results in depletion of protein molecules from all directions other than the sidewall. The depletion is greatest along the centerline direction, which has the largest potential energy disparities from that of the sidewall direction. As per Fig. 7A, at a critical DC field offset under NDEP conditions, the ensuing depletion can cause net preconcentration along the sidewall direction within a few microns from the constriction edge. For devices with larger constriction gaps, the potential energy disparities between the sidewall and centerline directions are lower, as in Fig. 6C, thereby resulting in lower preconcentration at the wider potential wells, as in Fig. 6D. This explains the experimental data indicating more uniform preconcentration along the centerline (in Fig. 3A) versus the sidewall direction (in Fig. 3B) for the 140-nm constrictions, as opposed to the larger differences along these directions for 50-nm constriction devices. It also causes a lower degree of depletion at larger constriction gaps (Fig. 7A versus Fig. 7B) and explains the lower extent of depletion zone in the experimental data of Fig. 2D (140-nm constriction) versus Fig. 2A (50-nm constriction). At subcritical DC fields, the potential wells are not deep enough to cause substantial preconcentration in comparison to the case where critical DC conditions are applied. This causes a lower degree of depletion and preconcentration as per the schematics in Fig. 7C. This is consistent with the experimental data in Fig. 2H, as well as more uniform preconcentration along the centerline versus sidewall (Fig. 3A and B) at conditions of subcritical DC (0.3 V/cm) versus critical DC field (1.5 V/cm). Hence, sub 100-nm constriction gaps enhance the energy barrier at

the constriction and create more disparities at the centerline versus sidewall direction of the device to enable narrow potential wells along the sidewall direction for rapid and steep degrees of protein preconcentration. A critical DC field offset to sufficiently tilt the potential profile coupled to significantly small constriction gaps is required to cause deep and narrow potential wells for protein preconcentration. Finally, a critical level of F_{NDEP}, which only occurs at the characteristic frequency of 1 MHz for streptavidin protein molecules, is required to localize the preconcentration region in the vicinity of the nano- constriction.

In conclusion, a methodology utilizing a balance of electrokinetic forces at nano-constriction devices is described for enabling steeply rising levels of preconcentration of streptavidin protein molecules within physiological media based on the following three requirements. First, a characteristic AC frequency of 1 MHz is required to enable trapping of the protein molecules under negative dielectrophoresis (NDEP) conditions using a 200 V_{pp}/cm field. Second, devices with approximately 50-nm constriction gaps are required to cause narrow potential energy wells along the sidewall direction of the device. Third, a critical level of DC field offset to the AC field (experimentally determined to be 1.5 V/cm for approximately 50-nm constriction gap devices) is required to sufficiently tilt the potential profile to cause deep potential energy wells for protein preconcentration. Under these conditions, an elliptical-shaped depletion zone of larger extent along the device centerline length axis (∼20 μm for ∼50-nm constriction gap devices) than other directions forms instantaneously around the constrictions to result in rapidly rising levels of protein preconcentration along the sidewall direction from the constriction. While protein preconcentration can occur at NDEP conditions within devices containing larger constrictions (up to ∼140 nm) and under conditions of lower DC field offset, the smaller disparities in the potential energy profile along the sidewall versus centerline directions cause depletion zones of smaller extent to result in a smaller rise in the degree of preconcentration over time. These protein preconcentration methodologies may be applied toward biomarker discovery, protein crystallization, and rare target sensing for early disease diagnostics.

This work was supported by Asian Office Aerospace Research & Development (#114083 to N.S.S., FA2386-12-1-4002 to C.F.C.) and National Science Council (ROC) 99-2112-M-001-027-MY3, and AS Program of Nanoscience and Nanotechnology (to C.F.C.), as well as AS Nano Core Facilities and travel support (NSF 0701505) for device fabrication.

The authors have declared no conflict of interest .

5 References

[1] Sheehan, P. E., Whitman, L. J., *Nano Letters* 2005, *5*, 803–807.

[2] Polaskova, V., Kapur, A., Khan, A., Molloy, M. P., Baker, M. S., *Electrophoresis* 2010, *31*, 471–482.

[3] Inglis, D. W., Goldys, E. W., Calander, N. P., *Angew. Chem. Int. Ed.* 2011, *50*, 7546–7550.

[4] Wang, Y.-C., Stevens, A. L., Han, J. Y., *Anal. Chem.* 2005, *77*, 4293–4299.

[5] Kim, S. M., Burns, M. A., Hasselbrink, E. F., *Anal. Chem.* 2006, *78*, 4779–4785.

[6] Lee, J. H., Song, Y. A., Han, J. Y., *Lab Chip* 2008, *8*, 596–601.

[7] Jones, T. B., *Electromechanics of Particles*, Cambridge University Press, Cambridge, New York, 1995.

[8] Morgan, H., Green, N. G., *AC Electrokinetics: Colloids and Nanoparticles*, Research Studies Press Ltd., Willis-ton, VT, USA, 2003.

[9] Pethig, R., *Biomicrofluidics* 2010, *4*, 022811.

[10] Chou, C. F., Tegenfeldt, J. O., Bakajin, O., Chan, S. S., Cox, E. C., Darnton, N., Duke, T., Austin, R. H., *Biophys. J.* 2002, *83*, 2170–2179.

[11] Chou, C.-F., Zenhausern, F., *IEEE Eng. Med. Biol. Magazine* 2003, *22*, 62–67.

[12] Swami, N., Chou, C.-F., Ramamurthy, V., Chaurey, V., *Lab Chip* 2009, *9*, 3212–3220.

[13] Chaurey, V., Polanco, C. F., Chou, C.-F., Swami, N. S. *Biomicrofluidics* 2012, *6*, 012806.

[14] Swami, N., Chou, C. F., Terbrueggen, R., *Langmuir* 2005, *21*, 1937–1941.

[15] Zheng, L., Brody, J. P., Burke, P. J., *Biosens. Bioelectron.* 2004, *20*, 606–619.

[16] Gong, J.-R., *Small* 2010, *6*, 967–973.

[17] Clarke, R. W., White, S. S., Zhou, D., Ying, L., Klenerman, D., *Angew. Chem. Int. Ed.* 2005, *44*, 3747–3750.

[18] Maruyama, H., Nakayama, Y., *Appl. Phys. Express* 2008, *1*, 124001:1241–1243.

[19] Agastin, S., King, M. R., Jones, T. B., *Lab Chip* 2009, *9*, 2319–2325.

[20] Lapizco-Encinas, B. H., Ozuna-Chacon, S., *J. Chromatogr. A* 2008, *1206*, 45–51.

[21] Nakano, A., Chao, T.-C., Camacho-Alanis, F., Ros, A., *Electrophoresis* 2011, *32*, 2314–2322.

[22] Holzel, R., *IET Nanobiotechnol.* 2009, *3*, 28–45.

[23] Clarke, R. W., Piper, J. D., Ying, L., Klenerman, D., *Phys. Rev. Lett.* 2007, *98*, 198102.

[24] Sin, M. L. Y., Gau, V., Liao, J. C., Wong, P. K., *J. Lab. Automat.* 2010, *15*, 426–432.

[25] Gao, J., Sin, M. L. Y., Liu, T. T., Gau, V. L. J. C., Wong, P. K., *Lab Chip* 2011, *11*, 1770–1775.

[26] Liao, K.-T., Chou, C.-F., *J. Am. Chem. Soc.* 2012, DOI: 10.1021/ja3016523.

[27] Gu, J., Gupta, R., Chou, C. F., Wei, Q., Zenhausern, F., *Lab. Chip.* 2007, *7*, 1198–1201.

[28] Ramos, A., Morgan, H., Green, N., Castellanos, A., *J. Phys,. D: Appl/ Phys.* 1998, *31*, 2338–2353.

[29] Chae, K., Lenhoff, A., *Biophys. J.* 1995, *68*(3), 1120–1127.

[30] Thwar, P. K., Lingerman, J. L., Burns, M. L. *Electrophoresis* 2007, *28*, 4572–4581.

Scaling analysis of constriction-based dielectrophoresis devices for trapping nanoscale bio-particles in physiological media of high-conductivity

Vasudha Chaurey[1], Ali Rohani[1], Yi-Hsuan Su[1], Kuo-Tang Liao[1,2], Chia-Fu Chou[2,*], Nathan S. Swami[1,*]

1 – Electrical & Computer Engineering, University of Virginia, Charlottesville, VA 22904;

2 – Institute of Physics, Academia Sinica, Taipei, Taiwan;

* - Corresponding Authors: nswami@virginia.edu; cfchou@phys.sinica.edu.tw; Fax #: (434) 924 8818

Keywords: Dielectrophoresis, Electrothermal flow, Joule Heating, Nanoanalysis, Proteins

Abbreviations: DEP (Dielectrophoresis), ET (electrothermal)

Number of words: 4000 (excluding Abstract, Title Page, and Figure Captions)

Scaling analysis of constriction-based dielectrophoresis devices for trapping nanoscale bio-particles in physiological media of high-conductivity

ABSTRACT

Selective trapping and pre-concentration of nanoscale bio-particles (size < 100 nm) is significant for the separation and high-sensitivity detection of biomarkers. Dielectrophoresis is capable of highly selective trapping of bio-particles based on their characteristic frequency response. However, the trapping forces fall steeply with particle size, especially within physiological media of high-conductivity where the trapping can be dissipated by electrothermal flow due to localized Joule heating. Herein, we investigate scaling of the device within an electrodeless dielectrophoresis geometry through the application of highly constricted microchannels coupled to the reduction of channel depth to explore the net balance of dielectrophoretic trapping force versus electrothermal drag force on bio-particles. While higher degrees of constriction enable dielectrophoretic trapping of successively smaller bio-particles within a short time, the electrothermal flow due to enhanced Joule heating within media of high conductivity can cause a significant dissipation of bio-particle trapping. The dissipative effect of the electrothermal drag force can be reduced through lowering the depth of the highly constricted channels to sub-micron sizes, which substantially reduces the degree of Joule heating, thereby enhancing the range of voltages and media conductivities that can be applied towards rapid dielectrophoretic pre-concentration of silica nanoparticles (~50 nm) and streptavidin protein biomolecules (~5 nm). We envision the application of these methodologies towards nanofabrication, optofluidics, biomarker discovery, and early disease diagnostics.

Keywords: Dielectrophoresis, Joule heating, Electrothermal flow, Nanoanalysis, Proteins

Scaling analysis of constriction-based dielectrophoresis devices for trapping nanoscale bio-particles in physiological media of high-conductivity

I. Introduction

High-sensitivity detection of rare numbers of biomarkers requires methodologies for selective pre-concentration of the biomarker within physiologically relevant media in the proximity of the sensor [1]. In comparison to chemical affinity methods based on antibody depletion [2], electrokinetic methods within micro- or nanofluidic devices, can achieve far higher degrees of pre-concentration due to the large volume reduction [3]. Dielectrophoresis (DEP) enables highly selective trapping of bio-particles based on the characteristic frequency response of the dielectric permittivity of the bio-particle versus that of the medium [4], [5], and it has been extensively applied towards sorting of somewhat similar sized biological cells with differing dielectric frequency response [6]. However, its application towards trapping 5-50 nm sized biomarkers requires structures such as insulator posts or dielectric constrictions to enhance the local field using an electrodeless dielectrophoresis scheme, to offset the steep fall in DEP trapping forces with particle size [7], [8], [9], [10], as demonstrated for trapping proteins [11], [12], [13], [14], [15] and fragments of ss-DNA [16], [17]. Biomarkers need to be trapped under room temperature conditions, within physiological media of neutral pH and high conductivity, to maintain their conformation and bio-functionality. Hence, while dielectric constrictions enhance dielectrophoretic trapping forces, they also cause a significant degree of Joule heating within media of high conductivity (>1 S/m) due to enhanced current densities at the high-field points [18], [19]. The resulting localized temperature rise can adversely affect biomarker functionality (such as causing protein denaturation) and the ensuing temperature gradients can cause electrothermal flow that dissipates dielectrophoretic trapping.

The generation term for electrothermal flow: $\sigma_m E^2$, where σ_m is media conductivity and E is the local electric field, acts over a significantly long-range, due to its indirect action on the particles through a drag force. The trapping force due to DEP, on the other hand, is highly localized at the constriction due to its dependence on ∇E^2. Hence, within the constriction device geometry, electrothermal flow acts to dissipate trapping under positive DEP, due to their opposing directions [9]; while under negative DEP conditions, it causes spreading of the trapping zone over a diffuse region, thereby reducing the degree of pre-concentration [11]. While the DEP trapping force scales as: ∇E^2, the low-frequency (< 1 MHz) Coulombic component of electrothermal flow scales as: $(\nabla T.E)\ E$; where ∇T is the temperature gradient [20]. Hence, a scaling analysis of the DEP force versus electrothermal drag force for varying trapping conditions (applied field and media conductivity) and device conditions (constriction ratio and channel depth) can lead to nanofluidic device designs that are optimized to enhance trapping over dissipation. In this current work, we study how scaling of the device geometry, media conductivity and applied voltage affect DEP forces, localized temperatures and the balance of DEP trapping (F_{DEP}) versus electrothermal drag force (F_{ET}) on nanoscale bio-particles.

II. METHODOLOGY

A. Device Geometry: The device geometry of a dielectric constriction is shown in **Figure 1**. For experiments, the constriction channels were either patterned on PDMS or etched into a quartz substrate and then bonded onto cover slip glass for imaging the DEP translation of fluorescently labeled streptavidin protein (52.8 kDa, Molecular Probes, Engene, OR) or ~50 nm silica nanoparticles (Corpuscular Inc., Cold Spring, NY) using an inverted microscope (Zeiss Observer A1). The depth of the channel is indicated for each of the results.

B. Device Modeling: We focus herein on the balance of dielectrophoresis trapping force versus electrothermal flow for microfluidic channel constriction ratios varied from 50x (500 μm reduced to 10 μm) to 5000x (500 μm reduced to 0.1 μm); media conductivity varied from: 0.1-10 S/m; and the applied field varied from: 100-400 V/cm. Finite element methods, using the ESI-CFD ACE+ software (ESI CFD, North America, Huntsville, Al) were used for the computations.

Dielectrophoresis: The constriction micro-channel device works on the principle that the highly insulating constriction material enhances the applied field at the constriction tip. The average steady-state dielectrophoretic force, F_{DEP}, on a homogeneous spherical particle with electrical permittivity ε_p, conductivity σ_p and radius *a* suspended in a fluid with electrical permittivity ε_m and conductivity σ_m in a non-uniform AC electric field E is given by [4]:

$$\vec{\mathbf{F}}_{DEP} = 2\pi a^3 \varepsilon_m \underbrace{\mathrm{Re}\left(\frac{\varepsilon_p^* - \varepsilon_m^*}{\varepsilon_p^* + 2\varepsilon_m^*}\right)}_{K_{CM}} \nabla E^2 \qquad \text{..(Eq. 1)}$$

Here, K_{CM} is the Clausisus-Mossotti factor which depends on the frequency (ω) of the applied electric field as: $\varepsilon^* = \varepsilon + \sigma/j\omega$. The DEP force is experienced by the polarized particles only under non-uniform electric fields; hence, it is proportional to the gradient (or spatial non-uniformity) of the square of the electric field. For computational simplicity, we herein assume that K_{CM} is ~1, even though the value can range from 0 to 1, for experimental positive DEP conditions.

Joule heating and temperature profile: Electrical conductivity of the fluidic media in the channel under the applied field during dielectrophoresis, leads to current flow and hence Joule heating, thereby causing a temperature rise. Since the electric field in the channel is not uniform, the

heating is also non-uniform. At steady state, heat generated in the system is equal to the heat dissipated. Thus the temperature profile can be computed as [5]:

$$k\nabla^2 T + \left\langle \sigma \left| \vec{E} \right|^2 \right\rangle = 0 \qquad \ldots \text{(Eq. 2)}$$

Where k is the thermal conductivity of the fluid, T the temperature and $\sigma|E|^2$ is the Joule heating term. Here the convection term of heat transfer is neglected owing to the micro-scale geometry of the device where thermal conduction is main mechanism of heat transfer.

Electrothermal force: Electrothermal flow is the body force (F_{ET}) experienced by the fluid in presence of an applied electric field due to localized anisotropic heating in the channel. Gradients in temperature in the channel give rise to gradients in the electrical properties of the media, namely conductivity and dielectric permittivity. For an incompressible fluid, this is [20]:

$$\vec{F}_{ET} = \rho\vec{E} - \frac{1}{2}\left|\vec{E}\right|^2 \nabla\varepsilon \qquad \ldots \text{(Eq. 3)}$$

Here, ρ is the charge density (as a result of temperature gradients), ε is the dielectric permittivity and $\vec{E}$ is the applied electric field. The first term on the right hand side of the equation is the Coulomb force (F_C) while the second term is the dielectric force (F_D). Since, the origin of these forces is in the temperature gradients, they can be simplified and expressed as the time averaged force per unit volume in terms of temperature gradients as [5]:

$$\left\langle F_{ET} \right\rangle = \underbrace{-\frac{1}{2}\left(\frac{1}{\sigma}\frac{\partial\sigma}{\partial T} - \frac{1}{\varepsilon}\frac{\partial\varepsilon}{\partial T}\right)\nabla T \cdot \vec{E}\,\frac{\varepsilon\vec{E}}{1+(\omega\tau)^2}}_{F_C} \underbrace{-\frac{1}{4}\left(\frac{1}{\varepsilon}\frac{\partial\varepsilon}{\partial T}\right)\varepsilon\left|\vec{E}\right|^2 \nabla T}_{F_D} \qquad \ldots \text{(Eq. 4)}$$

As apparent from the expression above, the electrothermal forces are frequency dependent. At low frequency, the Coulomb forces (F_C) are dominant while at high frequencies the Dielectric

forces (F_D) become dominant [20]. We focus on low frequency AC fields (< 1 MHz) within this work; hence, the dominant electrothermal force is the Coulomb force (F_C). As per [21], the temperature dependence of the conductivity and permittivity are given by $\frac{1}{\sigma}\frac{\partial\sigma}{\partial T} = 2\%$ and $\frac{1}{\varepsilon}\frac{\partial\varepsilon}{\partial T} = -0.4\%$. Hence, since: $\frac{1}{\sigma}\frac{\partial\sigma}{\partial T} - \frac{1}{\sigma\varepsilon}\frac{\partial\varepsilon}{\partial T} > 0$, the force direction can be estimated based on the sign of $\nabla T \cdot \vec{E}$. When the temperature gradient is parallel to the electric field, the Coulomb force is directed against the electric field and vice versa.

Electrothermal Flow Profile: Since the body force due to electrothermal flow acts to move the bulk fluid, it can be included within the Navier-Stokes equation. Thus, given the body force and assuming an incompressible fluid with low Reynolds number, the steady state Navier-Stokes equation can be written as:

$$\eta\nabla^2\vec{\mathrm{v}} - \nabla\mathrm{p} + \langle\vec{\mathrm{F}}\rangle = 0 \qquad \ldots \text{(Eq. 5)}$$

Here, η is the viscosity, p is the pressure and $\langle\vec{F}\rangle$ is the average volumetric force on the fluid. In this case $\langle\vec{\mathrm{F}}\rangle$ can be approximated as [22]: $\langle\vec{\mathrm{F}}\rangle = \langle\vec{\mathrm{F}}_{\mathrm{C}} + \vec{\mathrm{F}}_{\mathrm{D}}\rangle$. As the pressure in the fluid is constant and at low frequencies, electrothermal force is dominated by the Coulomb force, the equation is reduced to

$$\eta\nabla^2\vec{\mathrm{v}} + \langle\vec{\mathrm{F}}_{\mathrm{C}}\rangle = 0 \qquad \ldots \text{(Eq. 6)}$$

Balance of forces on the bio-particles: Finally, we examined the balance of $\vec{F}_{ET}$ versus $\vec{F}_{DEP}$ forces on the net mobility for the bio-particles for varying device conditions (constriction ratio and channel depth) and field conditions (applied field and media conductivity). The bulk fluid flow acts on the bio-particle in the form of drag force, thereby affecting the particle trajectory. Particle terminal velocity in the fluid can be given by:

$$\vec{v}_p = \vec{v}_f + \frac{\vec{F}_p}{\gamma}$$

…(Eq. 7)

Here, $\vec{v}_p$is the net particle velocity, $\vec{v}_f$ is the fluid velocity due to electrothermal flow, $\vec{F}_p$ is the force acting on the particle, which in this case is the dielectrophoretic force ($\vec{F}_p = \vec{F}_{DEP}$) and γ is the drag coefficient for the particle. Assuming a spherical particle of radius,a, the drag coefficient is given by:$\gamma = 6\pi\eta a$…(Eq. 8)

From this analysis, net force on the particle can be computed as:

$$\vec{F}_{pTotal} = \gamma\vec{v}_f + \vec{F}_{DEP}$$

…(Eq. 4

III. Results

III.1. Enhancing DEP trapping through scaling the constriction ratio: Based on the cubic dependence of the DEP force on the hydrodynamic radius of the particle (*a*), as per (Eq. 1), the DEP force decreases cubically with particle size. As per the device structure under the DEP field in Figure 1, an insulator constriction enhances the conduction current (at low frequencies) and displacement current (at high frequencies) within the constricted gap region of the device, thereby enhancing the density of field lines in the vicinity of the constriction edge to enable the localized enhancement of DEP trapping forces due to higher field (dependent on constriction ratio, R) and its gradient (dependent on sharpness of the constriction). We consider a field of 350 V/cm within channels containing constrictions with ratios (R) of 500x (500μm to 1μm) and 5000x (500μm to 0.1μm) for trapping bio-particles of sizes 50nm and 5nm, within media of 1 S/m conductivity. Comparing trapping forces to the Brownian motion on particles, the minimum DEP force to trap 50 nm and 5 nm particles can be determined as ~1 fN and ~3 fN, respectively,

as per Appendix A, whereas a significant degree of pre-concentration within minutes would require forces in the pN range [Soory]. From 錯誤! 找不到參照來源。 (a) and (c), it is clear that for 50 nm bio-particles, ~pN range DEP force distributions can be attained over a considerable extent of the constriction region for devices with 500x and 5000x fold constrictions. However, upon a one order of magnitude reduction in bio-particle radius (from a = 50 nm to 5 nm), the magnitude of the DEP force is lowered by 3 orders of magnitude. As can be seen from 錯誤! 找不到參照來源。(b), the regions of device with DEP force greater than ~pN are almost negligible for devices with 500x constrictions, whereas with 5000x constrictions in Figure 2(d), this region with > pN DEP trapping forces is restricted to the constriction edges. Since bio-particles under the effect of DEP force move with a velocity given by: $\vec{v} = \vec{F}/6\pi\eta a$, this reduction in force magnitude will in turn cause a reduction in particle trapping velocity and a proportionate increase in particle trapping time. Based on the magnitudes of the velocity profiles of Figure 2(e)-(h), we can estimate that instead of trapping times on the order of a minute for 50 nm bio-particles using 500x constrictions [16], the same constriction ratio would likely take 100's of minutes to achieve a similar degree of pre-concentration with 5nm bio-particles. This trend is substantiated by our experimental observations of streptavidin protein pre-concentration in Figure 3, showing that while a 1000-fold degree of pre-concentration can be obtained within ~20 seconds using 9000x constrictions (constriction from 30 µm to 50 nm in X and Y directions, and from 3 µm to 200 nm in Z direction, as described previously [12]), the same degree of pre-concentration would likely take tens of minutes using 3000x constrictions (constriction from 30 µm to 150 nm in X and Y directions, and from 3 µm to 200 nm in Z direction), and no perceptible pre-concentration can be observed with 1000x constrictions.

III.2. Constraints on scaling imposed by Joule heating: The chief constraint to scaling down the constriction gap (higher R) arises from Joule heating in the constriction region. In order to maintain the functionality of the bio-particle, such as conformations required for its participation within biochemical recognition events, the media conductivity (σ_m) needs to be in the range of 1-10 S/m (~50–500 mM salt levels). The application of DEP fields within media of high-conductivity causes an enhanced level of current flow, especially within devices containing dielectric constrictions to significantly enhance the electric field ($\vec{E}$). This causes Joule heating [23], which is proportional to: $\sigma_m|\vec{E}|^2$. Furthermore, the non-uniformity of the field in the constriction region versus elsewhere in the channel causes the Joule heating to be non-uniform. Additionally, since the floor and ceiling of the micro-channel act as the predominant heat sinks for the generated heat in the fluid through Joule heating, temperature gradients (∇T) are formed. A hot spot develops midway through the channel depth (5 μm), as shown in Figure 4a, where local temperatures can rise to 43.4°C (316.4K) for a 5000x constriction (500 to 0.1μm constriction) under 350 V/cm fields within media of 1 S/m conductivity. In Figure 4b we show evidence for the destruction of PDMS constriction tips due to significant levels of Joule heating, especially in the central region of channels of ~ 5 μm depth. These significant levels of Joule heating can cause the denaturation of proteins, and the resulting temperature gradients drive electrothermal flow in the bulk fluid. As discussed previously, such electrothermal flow can dissipate trapping under positive DEP conditions [9] and reduce the degree of pre-concentration under negative DEP conditions [11].

To understand the limits imposed by Joule heating on the range of applied voltages and media conductivity that can be applied towards dielectrophoretic trapping within devices containing highly scaled constriction ratios (large R), we present temperature simulations of the

hotspot region under these conditions. It is apparent here that the Joule heating causes a non-linear rise in the temperature with media conductivity (Figure 4c) and with applied field (Figure 4d). With 500x constriction devices of 5 μm depth, the temperature rises to just a few degrees above the ambient (300 K) for the voltages studied herein, as per Figure 4d. However, with 5000x constriction devices of 5 μm depth, the temperature rises sharply to several tens of degrees above ambient at fields > 250 V/cm within media of σ_m = 1 S/m (Figure 4d); and the temperature can rise to aqueous boiling point levels at σ_m = 10 S/m, even at 100 V/cm fields (Figure 4c). With decreasing channel depth (t), the generation term due to Joule heating can be significantly reduced due to the dependence of temperature at the hotspot (T_{max}) on the square of channel depth (t^2), based on a parallel plate capacitor model (Appendix B). Hence, a significant lowering of the temperature at the hotspot is apparent in Figure 4c and d.

III.3. Balance of dielectrophoretic trapping force versus electrothermal drag force: Temperature gradients within the constriction device can cause a significant level of electrothermal flow on the fluid, which can influence the overall particle trajectory and lead to increased drag force on the particles. In the vicinity of the hotspot region within the constriction (Figure 4a), the direction of electrothermal flow outwards away from the constriction opposes the direction of bio-particle trapping force under positive dielectrophoresis towards the constriction tip [9]. Hence, we analyze the influence of device scaling; i.e. the enhancement of constriction ratio (R) to enable trapping of smaller bio-particles and the reduction of channel depth (t) to reduce the Joule heating on the net balance of dielectrophoretic trapping force (F_{DEP}) versus electrothermal drag force (F_{ET}) on bio-particles. This balance of force will limit the range of electric fields and media conductivity that can be applied towards trapping nanoscale bio-particles (a ~ 5-50 nm), where large constriction ratios are required as per the results presented in

Figure 2. It should be noted that the dissipative action under F_{ET} is more long-range than the trapping action under F_{DEP}, due to the dependence of the latter on field gradients which are highly localized at the constriction tip. Furthermore, while F_{DEP} acts almost instantaneously on the polarized particles, F_{ET} requires a significant temperature gradient to set-in, which can take a longer time to reach steady state. These effects are apparent in Figure 5, which presents observations on the gradual dissipation of dielectrophoretic trapping under PDEP due to the ensuing electrothermal drag force on ~50 nm silica nanoparticles within conductive media (σ_m=0.5 S/m) and high fields (~350 V/cm). The peak dielectrophoretic trapping is reached within ~10 seconds (Figure 5a), at which point the dissipative action of F_{ET} lowers the degree of DEP trapping (Figure 5b-d). As per the fluorescence profiles in Figure 5e, beyond the peak DEP trapping time, electrothermal drag force causes the fluorescence intensity to gradually drop and the peak intensity is shifted closer to the left or right constriction tips, where F_{DEP} is highest, and away from the center of the constriction closer to the hotspot, where F_{ET} is highest.

As discussed previously, reducing the constriction channel depth (t) lowers the Joule heating and temperature of the hotspot at the center of the constriction (x, y, z = 0, 0, 0) (Figure 4c and 4d). However, in order for this to cause a lowering of F_{ET}, the ensuing drop in temperature difference between the hotspot and channel walls (which are close to ambient) should be sharper than the drop in channel depth (t), since F_{ET} depends on the temperature gradient (∇T=temperature difference / depth). It is apparent from Figure 6, within the plots of F_{ET} versus applied field (Figure 6a) and versus σ_m (Figure 6b), that F_{ET} is lowered with channel depth, especially at fields higher than 200 V/cm within media of σ_m = 1 S/m (Figure 6a); and at σ_m > 1 S/m at E=400 V/cm fields (Figure 6b). However, it must be noted that this drop in F_{ET} with depth is less sharp than the drop with depth of the respective temperature values at the

hotspot in Figure 4c and d, since F_{ET} depends ∇T. The greater degree of lowering of F_{ET} at successively lower channel depths (t) is apparent within the plot of F_{ET} versus channel depth in the inset of Figure 6b, where F_{ET} exhibits an exponential reduction at sub-μm channel depths, suggesting that significant gains to the balance of F_{DEP} versus F_{ET} can be realized. It is also apparent that F_{ET} depends non-linearly on the field (Figure 6a) and linearly on σ_m (if Figure 6b were plotted on a linear X-axis), as expected from its dependence on $\sigma_m E^2$.

Finally, we explore the trade-offs on the balance of F_{DEP} versus F_{ET} for the trapping of successively smaller bio-particles using successively higher constriction ratios (R). While the dielectrophoretic forces exhibit a cube-fold dependence on particle radius, the electrothermal drag force falls linearly with particle radius, as given by: $F_{Drag} = 6\pi\eta a\boldsymbol{v}$, where η is the fluid viscosity, a is the particle radius and $\boldsymbol{v}$ is the fluid velocity. Figure 7a summarizes this force balance in terms of the respective force magnitudes and Figure 7b summarizes it in terms of velocity magnitudes due to the respective forces, to eliminate the effect of F_{ET} on particle size. For a given bio-particle size, both the dielectrophoretic trapping forces and the electrothermal drag forces are observed to increase equivalently with increasing constriction ratios. However, with decreasing bio-particle size, F_{DEP} falls more sharply than F_{ET} due to its dependence as cube-fold rather than linear on particle size, thereby reducing the gap between the two forces at a given constriction ratio (R), and this is especially apparent at the smaller bio-particle sizes. Hence, while at a = 50 nm, F_{ET} values are insignificant due to the greater than 4 orders of magnitude lower F_{ET} versus F_{DEP}, at a = 5nm, the difference between the two forces is just two orders of magnitude at σ_m=1 S/m and E=400 V/cm, and the difference drops to less than one order of magnitude at σ_m=10 S/m and E=400 V/cm. Note that this analysis is based on a comparison of the maximum values of F_{ET} to F_{DEP}. Hence, this difference between the two forces

is likely to be further lowered if we had included the following within our analysis: (1) The more localized profile of F_{DEP} at the constriction tip in comparison to F_{ET}, due to the dependence of the F_{DEP} on field gradient; (2) The fall of F_{DEP} within media of higher conductivity (σ_m), due to changes in polarizability with decreasing (σ_p-σ_m) for the Clausius-Mossotti factor (K_{CM} in Eq. 1); (3) The lowered F_{DEP} due to the limited polarizability of bio-particles, such as ss-DNA and proteins, to result in K_{CM} below the unity value assumed within the calculations herein.

CONCLUSIONS: In this work we investigate the effect of scaling the constriction device geometry on the balance of dielectrophoretic trapping versus electrothermal drag force on nanoscale bio-particles (< 100 nm). Effective dielectrophoretic trapping of nanoscale bio-particles requires high constriction ratios; i.e. at least 500x for ~50 nm particles and 5000x for ~5 nm particles. However, within media of conductivities in the 1-10 S/m range, Joule heating causes temperature rise to several tens of degrees above ambient in the hotspot region at the midway depth point within the constriction region and the resulting electrothermal flow can cause a significant dissipation of the trapping of nanoscale bioparticles. Through reduction of the depth of the highly constricted channels to sub-micron sizes, the degree of Joule heating can be substantially reduced thereby significantly enhancing the range of applied voltages and media conductivity that can be applied to enable pre-concentration of silica nanoparticles (~50 nm) and streptavidin protein biomolecules (~5 nm).

ACKNOWLEDGEMENTS: This work was supported by Asian Office Aerospace Research & Development (#114083 to N.S.S., FA2386-12-1-4002 to C.F.C.) and National Science Council (ROC) 99-2112-M-001-027-MY3 and AS Program of Nanoscience and Nanotechnology (to C.F.C.). The authors have no financial or commercial conflicts of interest on this research.

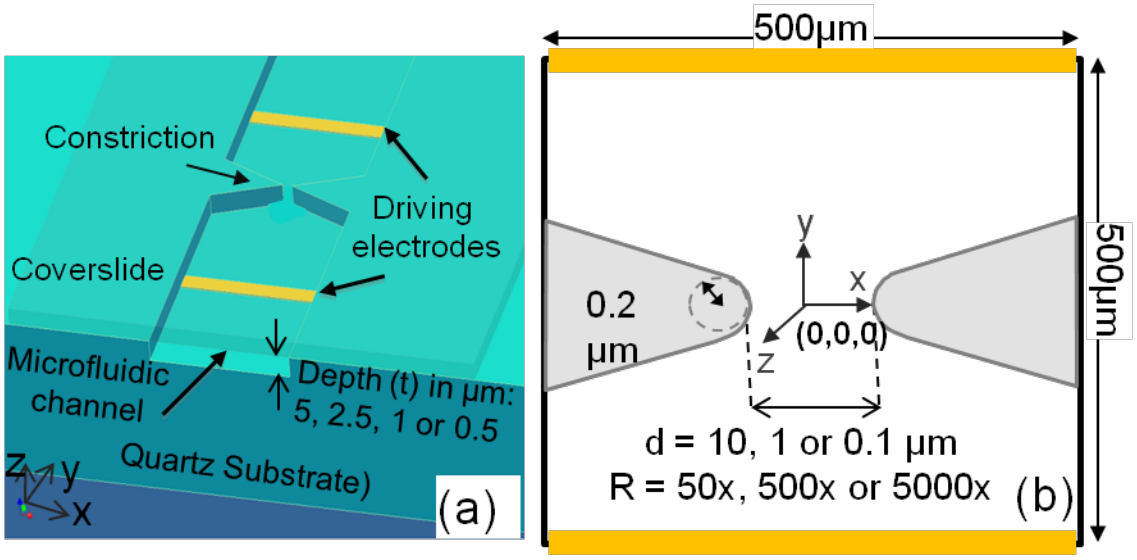

Figure 1(a) Device geometry for the insulator constriction in microfluidic channel. (b) Dimensions and coordinate system of the microchannel for the device modeling studies.

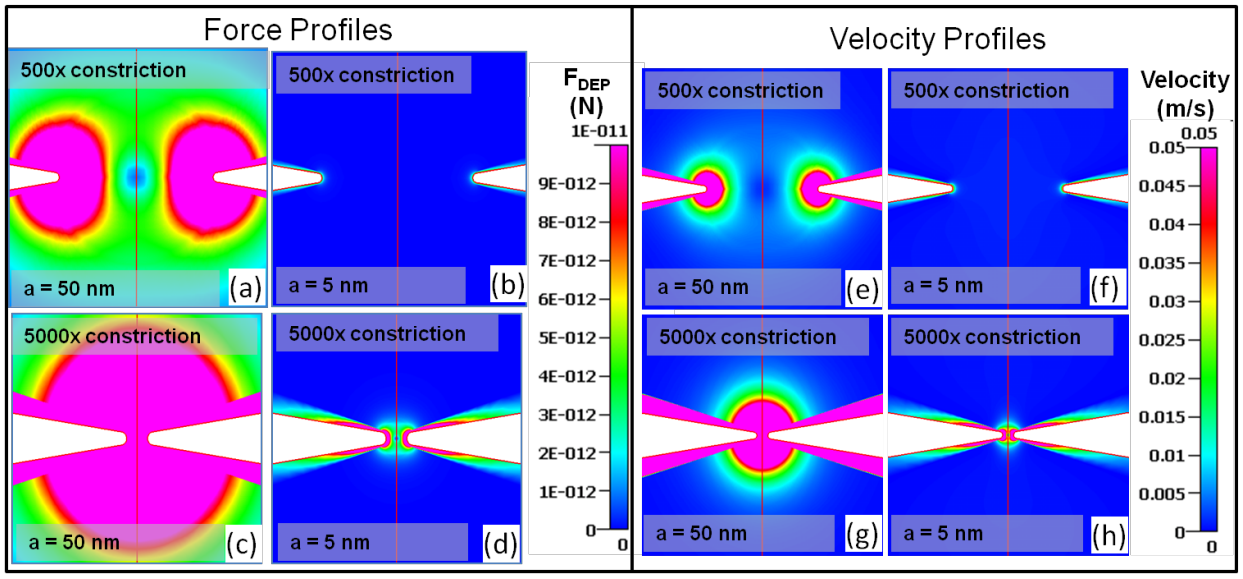

Figure 2: DEP force (a-d) and velocity profiles for constriction ratios of 500x (a-b and e-f, respectively) and 5000x (c-d and g-h) for trapping particles of hydrodynamic radius: a = 50 nm (a, c, e and g) and a = 5 nm (b, d, f, and h).

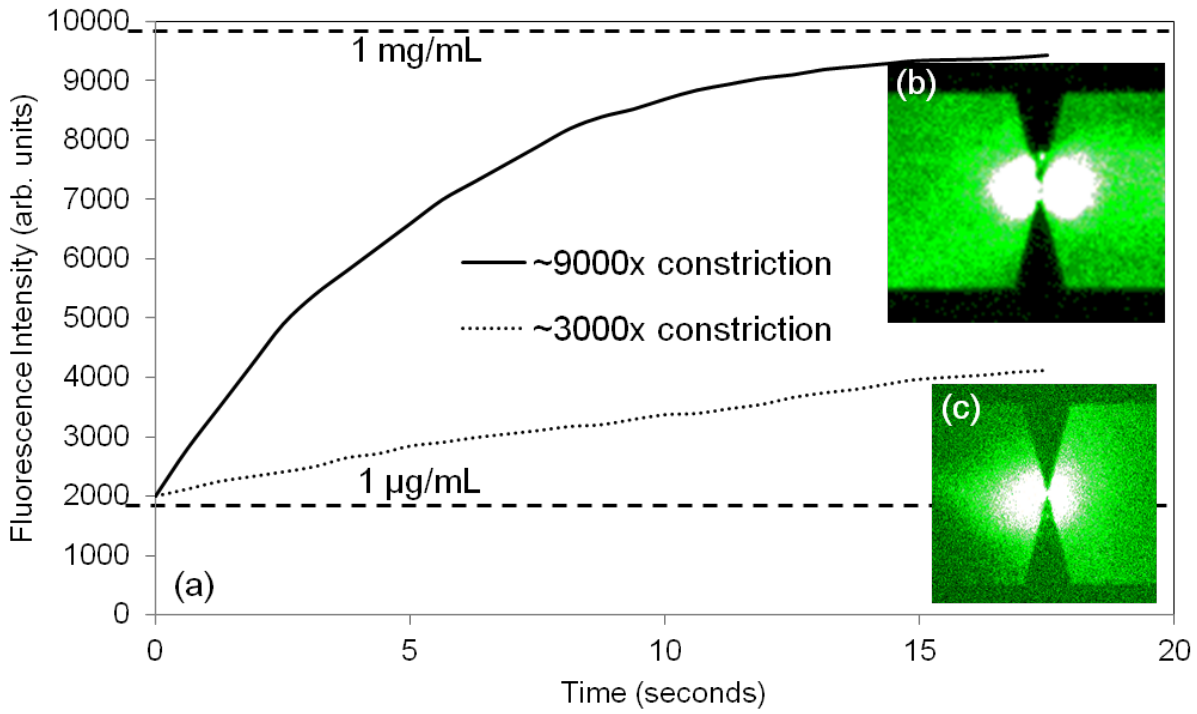

Figure 3: (a) Fluorescence intensity versus time for pre-concentration of fluorescently labeled (Alexa 488) streptavidin protein molecules in PBS buffer (~150 mM salt) using devices with constriction ratios of: (b) 9000x and (c) 3000x. The fluorescence intensity values corresponding to 1 µg/mL and 1 mg/mL concentration levels are shown. The device shows protein pre-concentration by positive dielectrophoresis at 100 kHz and fields of ~300 V_{pp}/cm. The channel depth is 200 nm for both the constriction ratios.

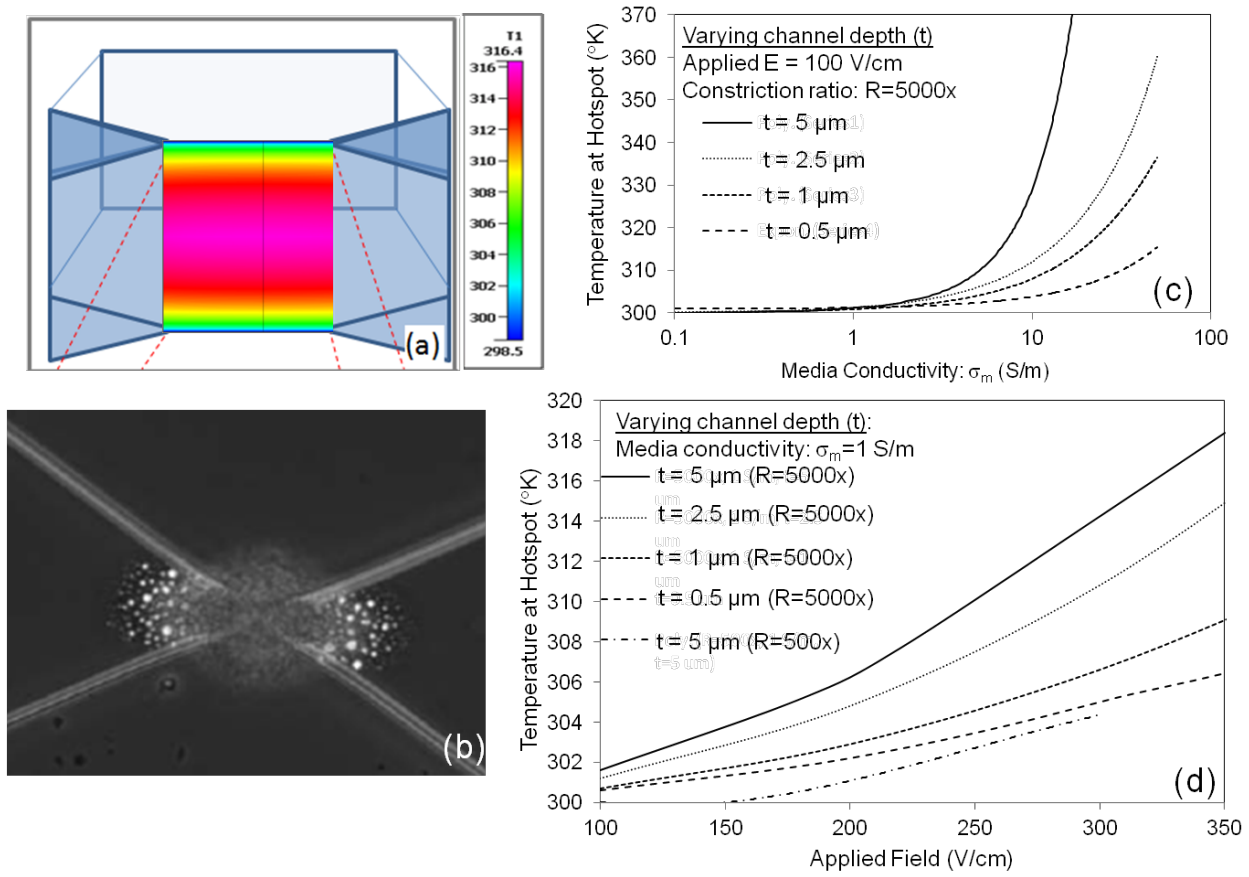

Figure 4: (a) Temperature profile across channel depth within the constriction region shows a hotspot midway through the channel. (b) Destruction of PDMS constriction tips due to Joule heating under ~400 V/cm fields with σ_m=0.5 S/m. The sharp rise in temperature at the hotspot with varying: (c) media conductivity (σ_m); and (d) applied field, can be lowered through reduction in channel thickness (t), especially within 5000x constriction ratio devices.

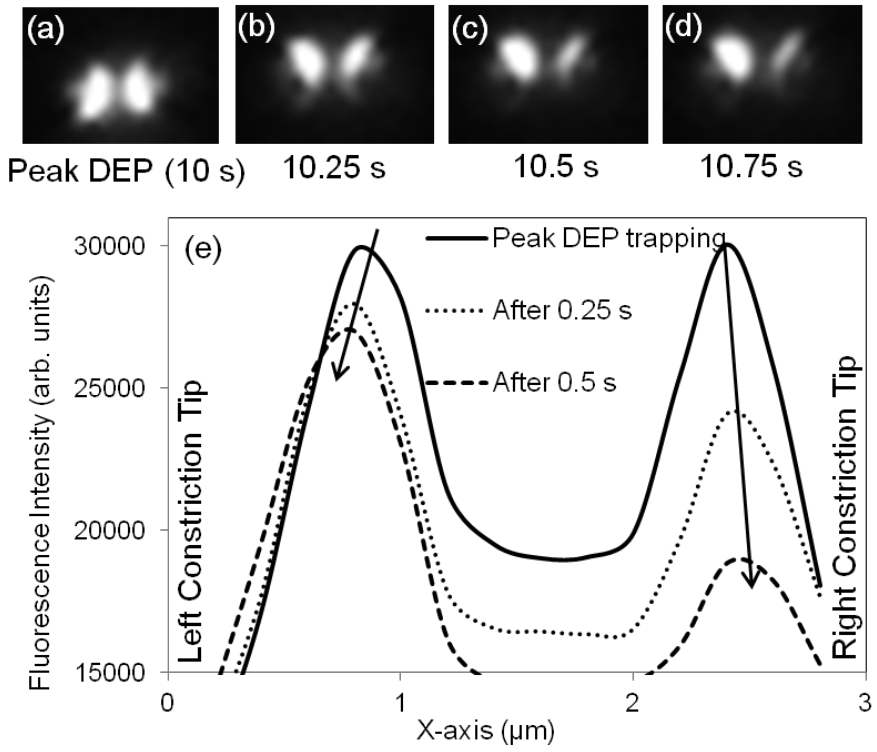

Figure 5: Dissipation of DEP trapping due to electrothermal flow is apparent within: (a) – (d) fluorescence images of the constriction tip region after peak DEP accumulation (~ 10s); and: (e) the fluorescence intensity profiles near the constriction tip.

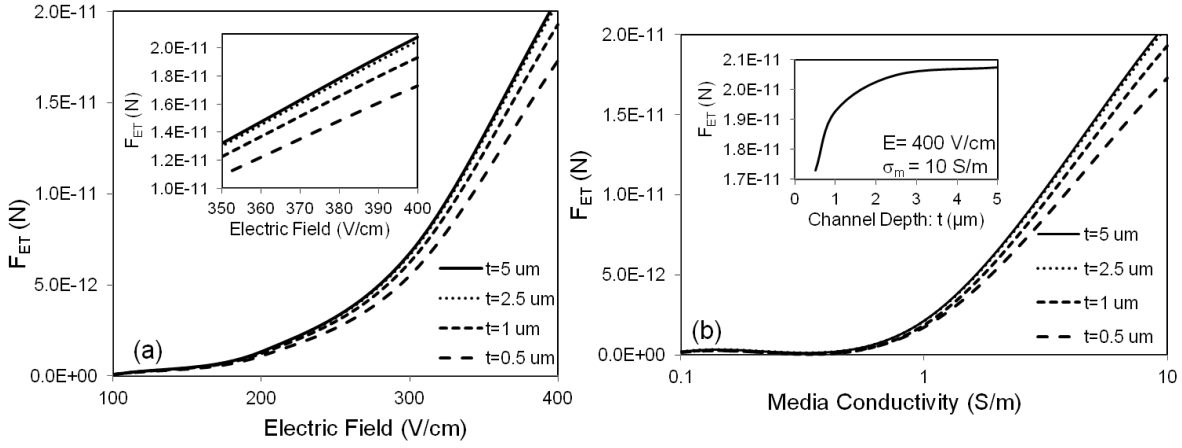

Figure 6: Rise of electrothermal drag force (F_{ET}): (a) quadratically with applied field (E), and (b) linearly with media conductivity (σ_m), can be reduced through lowering the channel depth (t). However, this reduction is less sharp than that of Joule heating with channel depth in Figure 4c

and d, due to the dependence of F_{ET} on temperature gradient (∇T). An exponential reduction in F_{ET} is apparent within the inset of (b) for sub-μm channel depths.

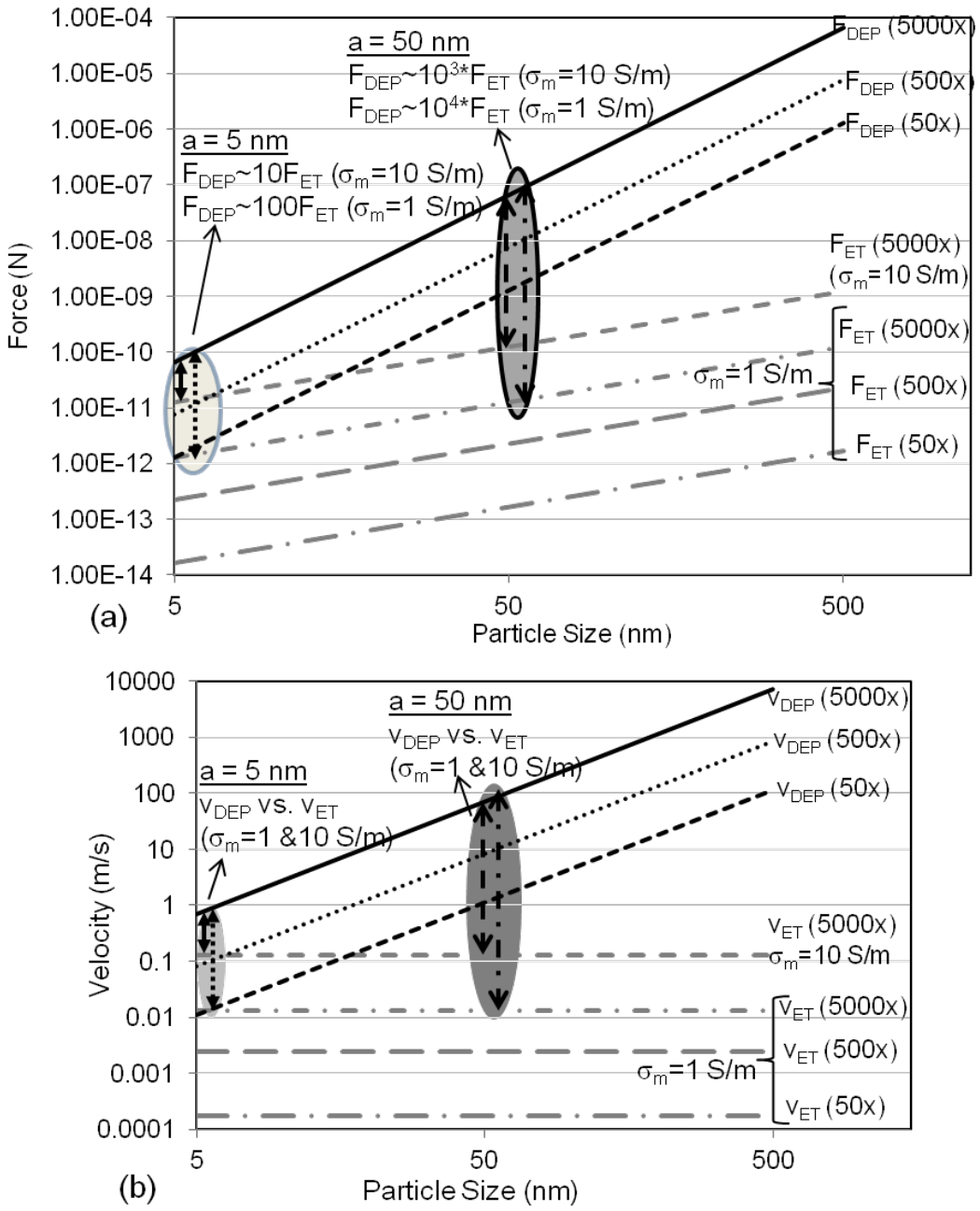

Figure 7: Balance of dielectrophoretic trapping forces versus electrothermal drag forces as a function of particle radius (a), constriction ratio (R) and media conductivity (σ_m), expressed as: (a) force on particles, and (b) velocity of particles under this force.

References

[1] P. E. Sheehan and L. J. Whitman, "Detection Limits for Nanoscale Biosensors," *Nano Letters,* vol. 5, no. 4, pp. 803-807, 2005.

[2] V. Polaskova, A. Kapur, A. Khan, M. Molloy and M. Baker, *Electrophoresis,* Vols. 471-482, p. 31, 2010.

[3] D. W. Inglis, E. Goldys and N. P. Calander, "Simultaneous concentration and separation of proteins in a nanochannel," *Angew. Chem. Int. Ed.,* vol. 50, pp. 7546-7550, 2011.

[4] T. B. Jones, Electromechanics of Particles, Cambridge, New York: Cambridge University Press, 1995.

[5] H. Morgan and N. G. Green, AC Electrokinetics: Colloids and Nanoparticles, Williston, VT, USA: Research Studies Press Ltd., 2003.

[6] R. Pethig, "Review Article—Dielectrophoresis: Status of the theory, technology, and applications," *Biomicrofluidics,* vol. 4, no. 2, pp. 022811-1-022811-35, 2010.

[7] C. F. Chou, J. O. Tegenfeldt, O. Bakajin, S. S. Chan, E. C. Cox, N. Darnton, T. Duke and R. H. Austin, "Electrodeless Dielectrophoresis of Single- and Double-stranded DNA," *Biophysical Journal,* vol. 83, pp. 2170-2179, 2002.

[8] C.-F. Chou and F. Zenhausern, "Electrodeless dielectrophoresis for micro total analysis systems," *IEEE Engineering in Medicine and Biology Magazine,* pp. 62 - 67 , 2003.

[9] V. Chaurey, C. Polanco, C.-F. Chou and N. Swami, "Floating electrode enhanced constriction dielectrophoresis for biomolecular trapping in physiological media of high conductivity," *Biomicrofluidics,* vol. 6, p. 012806, 2012.

[10] S. Srivastava, A. Gencoglu and A. Minerick, "DC insulator dielectrophoretic applications in microdevice technology: a review," *Analytical and Bioanalytical Chemistry,* vol. 399, pp. 301-321, 2011.

[11] K. Liao, M. Tsegaye, V. Chaurey, C. Chou and N. Swami, "Nano-constriction device for rapid protein pre-concentration in physiological media by electrokinetic force balance," *Electrophoresis,* vol. 33, pp. 1958-1966, 2012.

[12] K. Liao and C. Chou, *J. Am. Chem. Soc. Communications,* 2012.

[13] R. W. Clarke, S. S. White, D. Zhou, L. Ying and D. Klenerman, "Trapping of Proteins under

Physiological Conditions in a Nanopipette," *Angewandte Chemie International Edition,* p. 3747, 2005.

[14] B. H. Lapizco-Encinas, S. Ozuna-Chacon and Rito-Palomeras, *J. Chromatogr. A,* vol. 1206, p. 45–51, 2008.

[15] A. Nakano, T.-C. Chao, F. Camacho-Alanis and A. Ros, "Immunoglobulin G and bovine serum albumin streaming dielectrophoresis in a microfluidic device," *Electrophoresis,* vol. 32, p. 2314–2322, 2011.

[16] N. Swami, C.-F. Chou, V. Ramamurthy and V. Chaurey, "Enhancing DNA hybridization kinetics through constriction-based," *Lab on a Chip,* vol. 9, p. 3212–3220, 2009.

[17] N. Swami, C. Chou and R. Terbrueggen, "Two-potential electrochemical surface probe of DNA immobilization," *Langmuir,* vol. 21, pp. 1937-1941, 2005.

[18] M. L. Y. Sin, V. Gau, J. C. Liao and P. K. Wong, "Electrothermal Fluid Manipulation of High-Conductivity Samples for Laboratory Automation Applications," *Journal of Laboratory Automation,* vol. 15, pp. 426-432, 2010.

[19] J. Gao, M. L. Y. Sin, T. T. Liu, V. L. J. C. Gau and P. K. Wong, "Hybrid electrokinetic manipulation in high-conductivity media," *Lab on a Chip,* vol. 11, pp. 1770-1775, 2011.

[20] A. Ramos, H. Morgan, N. Greenz and C. A., "AC electrokinetics: a review of forces in microelectrode structures," *Journal of Physics D: Applied Physics,* vol. 31, pp. 2338-2353, 1998.

[21] CRC, CRC Handbook of Chemistry and Physics, 74 ed., L. D. R, Ed., London: CRC, 1994.

[22] A. Castellanos, A. Ramos, A. Gonz´alez, N. G. Green and H. Morgan, "Electrohydrodynamics and dielectrophoresis in microsystems: scaling laws," *Journal of Physics D: Applied Physics,* vol. 36, p. 2584–2597, 2003.

[23] B. Burg, V. S. Bianco and D. Poulikakos, "Electrokinetic framework of dielectrophoretic deposition devices," *Journal of Applied Physics,* vol. 107, pp. 124308-1-124308-11., 2010.

[24] K. Liao, M. Tsegaye, V. Chaurey, C. Chou and N. Swami, *Electrophoresis,* 2012.

[25] R. W. Clarke, S. S. White, D. Zhou, L. Ying and D. Klenerman, "Trapping of Proteins under Physiological Conditions in a Nanopipette," *Angewandte Chemie International Edition,* p. 3747, 2005.